The

ENGINEERS' DIGEST

REVIEW OF ENGINEERING PROGRESS ABROAD

MAY 1 0 1945

OL. VI. No. 3 MARCH, 1945

ERING
ARY

In addition to all their other advantages, CHURCHILL Precision Roll Grinders are easily operated.

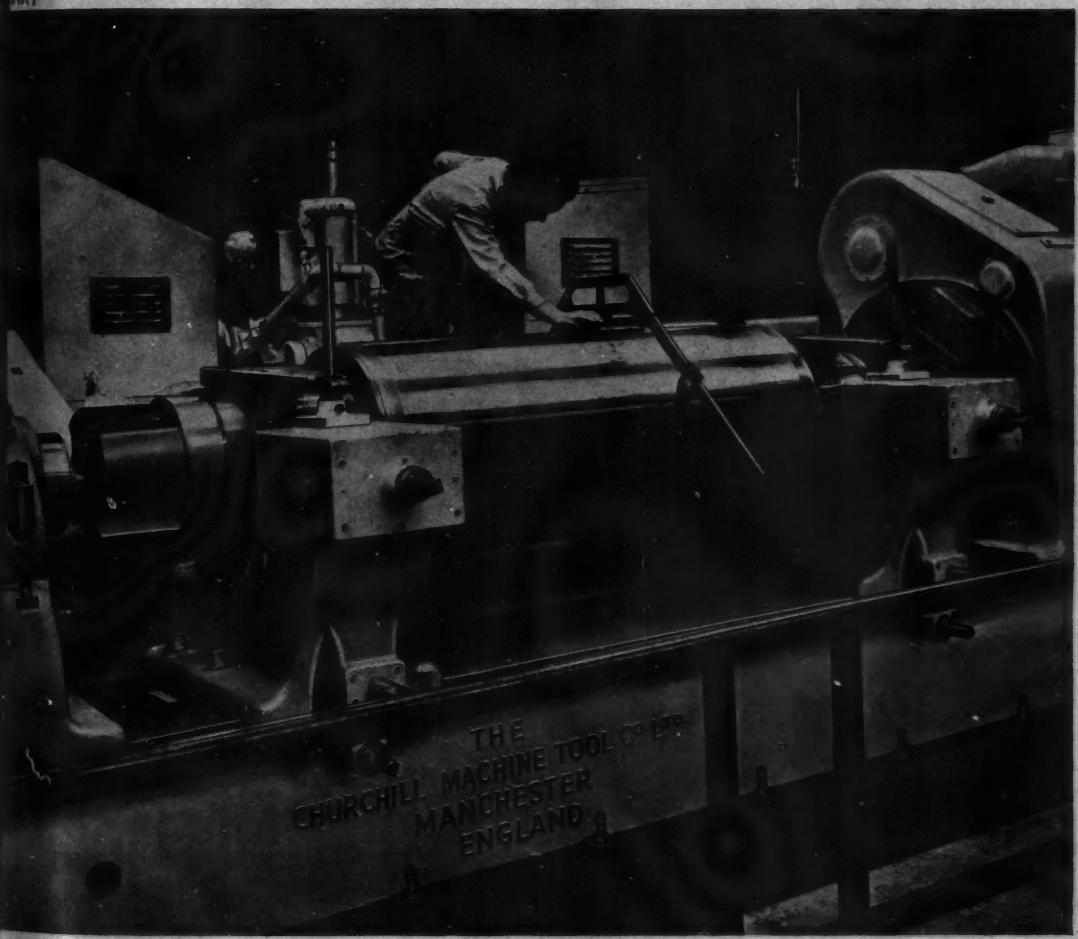

THE CHURCHILL MACHINE TOOL CO. LTD., BROADHEATH, Nr. MANCHESTER.

THE ENGINEERS' DIGEST

REVIEW OF ENGINEERING PROGRESS ABROAD

Published Monthly at 120, Wigmore Street, London, W. 1.

Publishers : **ENGINEERS' DIGEST LTD.** – – – – – – Telephone : WELBECK 9357

Adverstisement Dept. – 120, Wigmore Street, London, W.1. – – Telephone : Welbeck 9357

Distribution – – E. & F. N. SPON, LTD., 57, Haymarket, London, S.W.1.
Telephone : Whitehall 1860. Telegrams : Fenspon, Lesquare, London

Editorial Dept. – – 120, Wigmore Street, London, W.1. – – Telephone : Welbeck 9357

Subscriptions to : ENGINEERS' DIGEST LTD., 120, Wigmore Street, London, W.1, or
E. & F. N. SPON, LTD., 57, Haymarket, London, S.W.1.

ANNUAL SUBSCRIPTION OF 12 NUMBERS, £2 2s. SINGLE COPIES, 4s. 6d.

ADVISORY COMMITTEE

J. F. ALCOCK, B.A., A.M.I.Mech.E.
R. W. ALLOTT, M.A., A.R.Ae.S.
E. ALTON, D.Eng., A.M.Inst.B.E.
H. H. ASBRIDGE, M.B.E., M.I.Mech.E.
R. W. AYERS, M.I.W.
Col. J. BOWDEN, M.Inst.C.E., M.I.Mech.E.
H. H. BROUGHTON, M.I.Mech.E.
F. BUCKINGHAM, B.Sc., A.M.Inst.C.E., A.M.I.Mech.E.,
T. H. BURNHAM, B.Sc. (Lond.), A.M.I.Mech.E. [A.M.I.E.E.
J. S. CASWELL, M.Sc., M.I.Mech.E.
G. C. SAFFERY COOPER.
J. DICK, Ph.D., B.Sc., A.M.I.Mech.E.
D. FIFE, M.I.Mech.E.
G. E. FOXWELL, D.Sc. (Lond.), F.Inst.P., F.Inst.F.,
R. GRIFFITHS, M.Sc. [M.Inst.Gas.E.
H. HEYWOOD, Ph.D., M.Sc. (Eng.), A.M.I.Mech.E.
O. HURST, M.Inst.N.A.
Capt. J. S. IRVING, M.I.Mech.E., M.I.A.E., A.F.R.Ae.S., M.S.A.E.
F. C. JOHANSEN, M.Sc. (Eng.), M.I.Mech.E., F.R.Ae.S., M.I.Loco.E.
W. J. KEARTON, D.Eng., M.I.Mech.E., A.M.Inst.N.A.
Prof. W. KERR, Ph.D., M.I.Mech.E.
G. V. LOMONOSOFF, Dr.Ing., M.I.Mech.E.
B. J. LYMER, M.I.Mech.E.
D. T. MacIVOR, M.I.Mech.E., M.Cons.E.
W. O. MANNING, F.R.Ae.S.
R. B. MATTHEWS, Wh.Ex., A.M.Inst.C.E., M.I.E.E., F.R.Ae.S.
Prof. A. L. MELLANBY, D.Sc., LL.D., M.I.Mech.E.
J. H. R. RATCLIFFE, B.Sc. (Eng., Hons.), M.I.Mech.E.
Col. C. W. D. ROWE.
W. A. SCOBLE, D.Sc., A.R.C.Sc., M.I.Mech.E.
P. W. SEEWER, D.E. (Zurich), M.Inst.C.E., M.I.Mech.E.
Prof. S. PARKER SMITH, D.Sc., M.I.E.E., A.M.Inst.C.E.
C. F. H. VERITY, A.M.Inst.C.F., A.M.I.E.E., A.M.I.Mech.E.
E. G. WALKER, F.C.G.I., B.Sc. (Eng.), M.Inst.C.E., M.I.Mech.E., M.Am.Soc.C.E.
Major F. L. WATSON, M.Inst.C.E., M.I.Mech.E.
G. WATSON, M.Inst.C.E., M.I.Mech.E.
C. H. WOODFIELD, M.I.Mech.E., M.I.Struct.E.
T. WRIGHT, Ph.D., M.Sc.
M. L. YATES, Ph.D., M.Sc.Tech., M.A. (Com.), M.I.Mech.E.

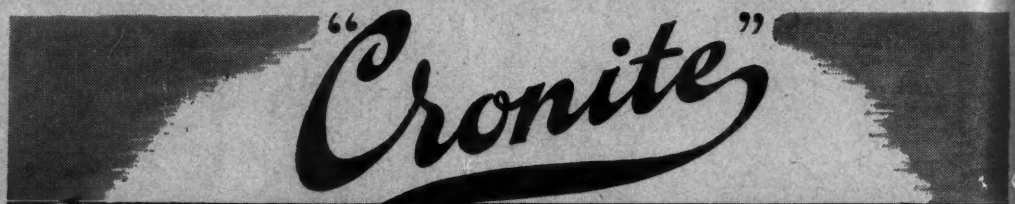

"CRONITE" is the Nickel Chromium Alloy of highest commercial grade. "CRONITE" castings find employment in almost every branch of the engineering industry replacing iron or steel for heat resisting purposes. There is no structural breakdown with the alloy, retention of shape being maintained almost to melting point.

Typical Uses at 800° Centigrade and over.

CASEHARDENING VESSELS.
ROTATING CARBURIZING RETORTS.
LEAD POTS.
SALT BATH VESSELS.
MUFFLES AND FURNACE PARTS.
FURNACE HEARTH PLATES.
GLASS BLOWER NOZZLES.
PYROMETER PROTECTION SHEATHS.

THE CRONITE FOUNDRY CO. LTD.
Lawrence Rd. Tottenham. London N15.

Telephone: STAMFORD HILL 4237

Ac
Br
Co
Ec
En
En
In
Lu
Th
Te
A
Top
The
3744

CONTENTS

page

Adsorption of Gases by the Steel Walls of Vacuum Discharge Apparatus and its bearing on the Life of Pumpless Mutators 81
" *The Engineers' Digest*," *Vol.* 6, *No.* 3, *p.* 81.

Braking Airscrew and High Speed Flight 77
" *The Engineers' Digest*," *Vol.* 6, *No.* 3, *p.* 77.

Comparison of Surface Roughness of Highly Finished Planes Surface 62
" *The Engineers' Digest*," *Vol.* 6, *No.* 3, *p.* 62.

Economic Characteristics of the High Speed Diesel Engine 71
" *The Engineers' Digest*," *Vol.* 6, *No.* 3, *p.* 71.

Energy Consumption of Hot Rolling 57
" *The Engineers' Digest*," *Vol.* 6, *No.* 3, *p.* 57.

Engine, Man, Animal and Plant 69
" *The Engineers' Digest*," *Vol.* 6, *No.* 3, *p.* 69.

Industrial Dust Separation and its Physical Principles 66
" *The Engineers' Digest*," *Vol.* 6, *No.* 3, *p.* 66.

Luminous Intensity of Arc Lamp Reflectors 63
" *The Engineers' Digest*," *Vol.* 6, *No.* 3, *p.* 63.

The Recovery of Hard Metal from Grinding Dust and Grinding Sludge 79
" *The Engineers' Digest*," *Vol.* 6, *No.* 3, *p.* 79.

Testing Non-ferrous Metals by New Magneto-Inductive Method 67
" *The Engineers' Digest*," *Vol.* 6, *No.* 3, *p.* 67.

ACTARC SUREARC

Hints on ARC WELDING

5

REINFORCING (3)

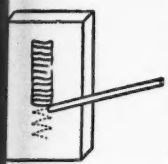

VERTICAL reinforcing is the most difficult to do. It will be seen that when welding from the top downwards, the molten metal tends to run down and does not bind with the parent metal. This can be prevented by pointing the electrode slightly downwards; a weld done in this fashion is called a wash-over.

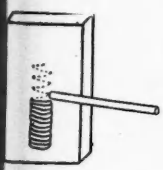

For a better job and also to put on a heavier reinforcing, it is usual to weld from the bottom upwards, the current in this case being somewhat reduced. This is because you are welding on to hot metal. The method is to use a weave as shown in diagram.

Top—down hand. Bottom—up hand.

There is an Actarc or Surearc Electrode for every job.

6

FILLET WELD

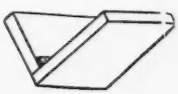

A RUN is laid down in the angle, using no weave and as short an arc as possible. The second run is, if necessary, made in a similar fashion. The finishing or top run is made with a weaving movement so that the weld will have a tidy appearance.

The lower illustration shows an upright fillet weld, made as before. Hold the electrode at an angle of 45 deg. to the horizontal, this enables the slag to be forced back over the weld metal.

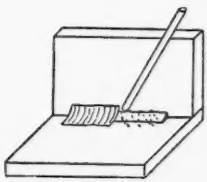

Actarc and Surearc plant and electrodes stand for economic welding.

ARC MANUFACTURING CO., LTD.

PROPRIETORS OF THE SUREARC ELECTRODE CO., LTD.

ACTARC WORKS, GOLDHAWK ROAD, LONDON, W.12.

Telephone : SHE 1151/3. Telegrams : Activarc, Phone, London

3744

ESC
SMALL
TOOLS
We are now in a position to give easier deliveries of Milling Cutters, Twist Drills, Ground Thread Hobs, Round or Square Tool-Bits and Escaloy Cemented Carbide for high-speed cutting.
ENGLISH STEEL CORPORATION LTD
OPENSHAW — MANCHESTER

ENERGY CONSUMPTION IN HOT ROLLING

By G. WALLQUIST. (From *Jernkontorets Annaler*, Vol. 128, 1944, pp. 249-306, 309-369).

IN modern rolling technique it is of considerable importance to be able to compute the specific energy consumption in KW hr. per ton of material rolled, the power requirements in KW or h.p., and also the required turning moment in ton-m. Knowledge of these data makes it possible not only to determine the size of rolling mill drive required for a new mill installation, but also to ascertain the production limits of an existing mill; it further enables the computation of the stresses to which the various components of the mill train are subjected and the study of the influence of the employment of different types of roll bearings upon the energy consumption of the mill.

To be able to carry out such computations, it is necessary to know the influence of the various operational factors upon the energy consumption. A determination of these various factors cannot be carried out on the basis of a purely theoretical mathematical speculation, but full account must be taken of actual test results. Reference is, therefore, mad in this report to actual tests made and operating experiences encountered in Sweden and in other countries.

Generally the energy requirements of the hot rolling process are expressed by the number of KW hours consumed per ton of material rolled, including both the actual work W performed by the roll mill drive and its losses. The total power consumption per ton of material is, therefore, given by

$$L_{tot} = \frac{W_{kl}}{3{,}600 \cdot G} = \frac{W_t + W_v}{3{,}600 \cdot \eta_{med} \cdot G}$$

where W_{kl} is the energy in KWsec supplied to the mill drive during a certain rolling time, W_t is the corresponding energy in KWsec represented by the idling losses, W_v is the energy expended upon the rolling process proper, η_{med} is the average efficiency of the drive during the working period considered, and G is the weight of material rolled during that period.

From the scientific point of view it would of course be more correct to define the energy consumption as the amount of energy required in carrying out the deformation of the material alone. Actually this energy cannot be measured by itself, and rolling energy requirements must, therefore, be determined as the sum total of rolling energy W_v and friction losses. In order to arrive at a figure for the energy consumption of the rolling process carried out in a number of passes, the concept of *specific rolling energy* is introduced, and this if given either in KW hours per ton of steel rolled or in kg m per unit volume of deformation produced. For a given number of passes the specific rolling energy can therefore be expressed either by $L_{v\,tot} = \frac{W}{3{,}600 \cdot G}$ in kW hours per ton of steel rolled or by $L_v = 102 \cdot \frac{W_v}{V_d}$ where V_d is the volume in cm³ of material displaced per roll pass. For a series of passes it can therefore be written

$$L_{v\,med} = 102 \cdot \frac{\Sigma_1 W_v}{V_{dx}}$$

where $\Sigma_1 W_v$ is the sum total of rolling energy consumed in the passes No. 1—X and V_{dx} is the total deformation of material which the material has undergone when it is discharged from roll pass No. X.

The concept of deformation or displaced volume was introduced by E. Kirchberg as far back as 1906; he defined it as the difference between the sectional area of the billet before and after the pass multiplied by the length of the billet, that is $V_d = (A_f - A_e)\, l_f$. In this expression A_f denotes the cross sectional area in mm² of the billet as it exists before the pass and A_e the corresponding area after the pass; while l_f is the length of the billet in mm. If the deformed volume is based upon the length l_e of the billet as it leaves the pass, it becomes

$$V_d = (A_f - A_e)\, l_e = (A_f - A_e) \frac{A_f}{A_e} \cdot l_f.$$

This expression yields greater numerical values than that based upon the original length of the billet.

More satisfactory in mathematical respects are the expressions for the volume deformation given by C. Kiesselbach and C. Hulst, which read

$$V_d = V \cdot 1n \frac{A_f}{A_e}$$

and Kiesselbach's parabolic formula

$$V_d = V \cdot 1n \sqrt{\frac{A_f - A_e}{A_e}}$$

in which V is the volume of the billet in cm³. But the latter expressions cannot be considered as sufficiently simple for practical applications, and the author, therefore suggests the formula $V_d = (A_f - A_e) \frac{l_f + l_e}{2}$ in which the specific rolling energy is seen to be based upon the mean of initial and final length of the rolled piece. This expression is used as basis in the evaluation of the test results discussed below.

The energy consumption incurred in the rolling of blooms was investigated in three blooming mills, AI, BI, and CI, of which AI and BI are equipped with two-high reversible mills and CI with three-high mills. The principal data of these mills are:

AI Blooming mill with reversible two-high train of three stands, Roll diameters 750-700 mm., babbitted roll bearings, Ilgner-Leonard drive.

BI Blooming mill with reversible two-high train of two stands, Roll diameters 770-705 mm., roller bearings, Ilgner-Leonard drive.

CI Blooming mill with three-high train of four stands, Roll diameters of 750-700 mm., babbitted roll bearings, Three-phase-induction motor.

Mill AI. This mill is furnished with an Ilgner-Leonard set of 600 r.p.m. synchronous speed and 1240 h.p. continuous capacity. (The d.c. generator is rated at 1680 KW continuous capacity at 560 volts.). This set is equipped with a 24 ton flywheel of 55,000 h.p. sec. The d.c. motors of the mill train total 2050 h.p. cont. and 6300 h.p. max. duty. The rolls of the first two stands are 1740 and 2070 mm. long in the body respectively. The tables are of the stationary type with a built-in manipulator before the first stand, while turning between the passes is done by hand. The rolls of the first stand were made of forged plain 0.7 per cent carbon material, and prior to the rolling tests had been in use for two weeks out of a normal service life of eight weeks.

TABLE 1.

Steel	Ingot		Composition of steel, %								
No.	Size, mm.	Weight, kg.	C	Si	Mn	P	S	Cr	Ni	Mo	Cu
A1	345 × 345	737	0.07	—	0.32	0.005	0.035	—	—	—	0.15
A2	345 × 345	701	0.13	—	0.34	0.011	0.036	—	—	—	0.14
A3	398 × 398	1,170	0.32	0.28	0.74	0.021	0.066	—	—	—	—
A4	398 × 398	1,186	0.59	0.27	0.45	0.029	0.030	—	—	—	0.14
A5	362 × 362	769	0.78	0.31	0.38	0.023	0.015	—	—	—	—
A6	362 × 362	752	1.28	0.12	0.30	0.021	0.012	—	—	—	—
A7	362 × 362	773	1.05	0.17	0.30	0.021	0.011	0.56	—	—	—
A8	362 × 362	765	0.93	0.33	0.41	0.022	0.013	1.02	—	—	—
A9	362 × 362	763	0.97	0.33	0.31	0.020	0.010	1.46	—	—	—
A10	345 × 345	665	0.07	0.48	0.56	—	—	17.7	8.95	0.09	—

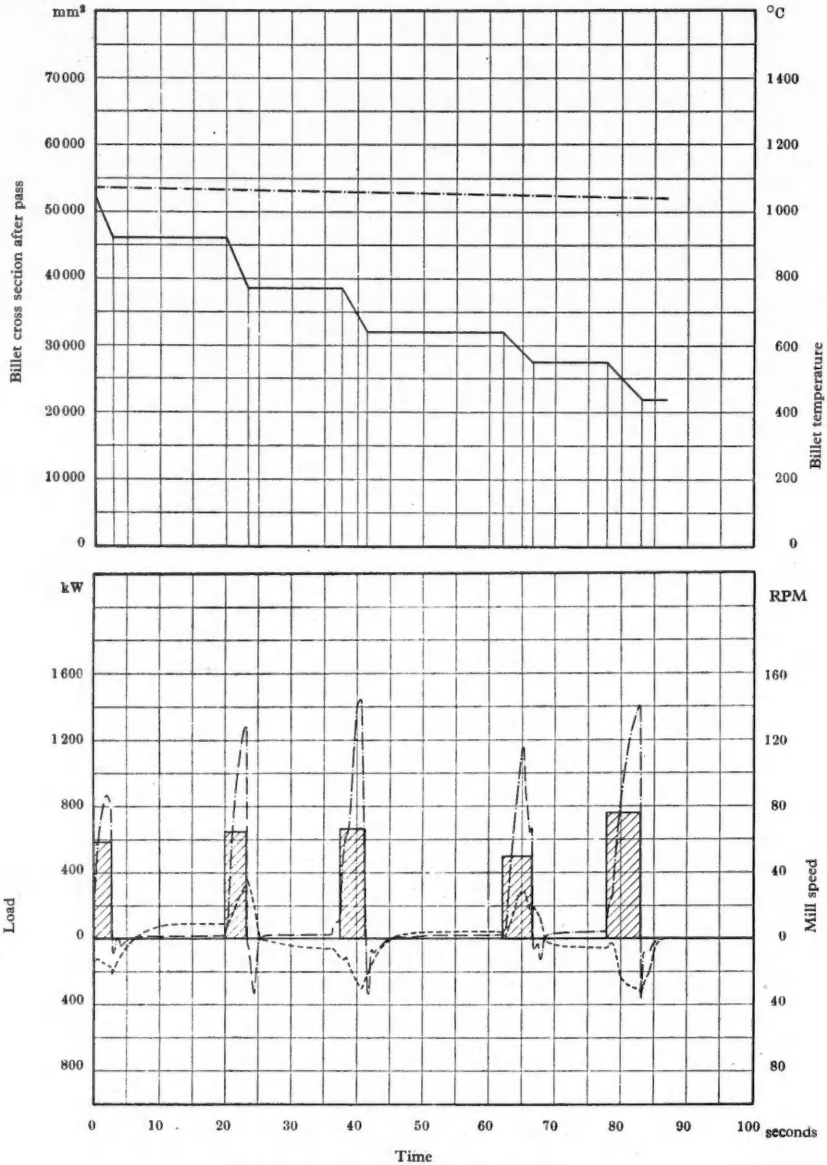

Mill A I with open-box passes rolling steel A_8.

Fig. 1. **Billet reduction and temperature diagram.**

Fig. 2. **Mill power consumption and mill speed diagram.**

In the tests the various steels were rolled with the same reduction, assuming identical passes for the various steel qualities. This is not strictly correct, since the spring of the mill as well as the spread depend upon the properties of the steel. The error introduced by this assumption is not, however, important, and affects only the specific rolling energy L_v per pass and not the mean value $L_{v\,med}$ or the total value $L_{v\,tot}$.

Table 1 shows the steels which were investigated.

The diagrams showing reduction, temperature, energy consumption, and roll speed obtained with steel A_2 are given in Figs. 1 and 2; while Fig. 3 shows the total specific rolling energy $L_{v\,tot}$ in KW hours per ton versus the elongation produced.

Mill BI.—This is a 770 mm. mill of recent construction equipped with Bibby coupling and two roll stands with roller bearings. The Ilgner-Leonard set consists of a 750 r.p.m. synchronous motor supplied at 6,000 volts, and having a continuous rating of 1350 h.p. It is equipped with an 8.2 ton flywheel of 52,000 h.p. sec. The d.c. generator of the set is a 460 volt machine with a continuous capacity of 1450 KW. The mill motors are designed for a supply voltage of 440 volt, 1750 KW cont. rating, 4200 KW max. rating and 75 ton. m., their speed range being 0-80 r.p.m. The rolls of the first stand have open box passes and those of the other stand have gothic and diamond passes. The body length of the rolls is 2,100 mm. throughout. A pair of roll bearings is shown in Fig. 4.

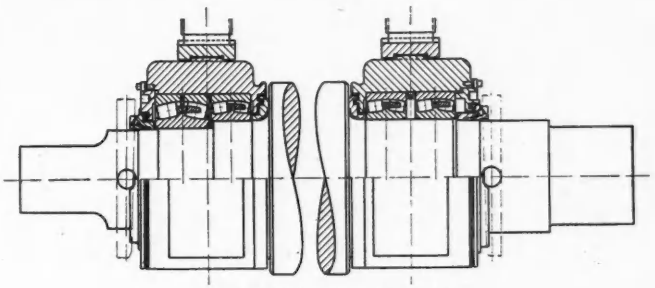

Fig. 4. **Roll bearings of mill B I.**

The first stand is equipped with approach tables and guides, while the second stand has a travelling table with built-in manipulator for turning the ingot between the passes.

The investigation was carried out with the employment of pearlitic rolls, which prior to the test had been in use only for a few weeks out of a total service life of six weeks in three-shift operation. Table 2 shows the steels rolled.

The values for $L_{v\,tot}$ ascertained in the various test runs are charted in Fig. 5 as function of the elongation produced.

Mill CI.—Mill CI is an old 750 mm. mill which was modernised two years ago. It consists of a three-high

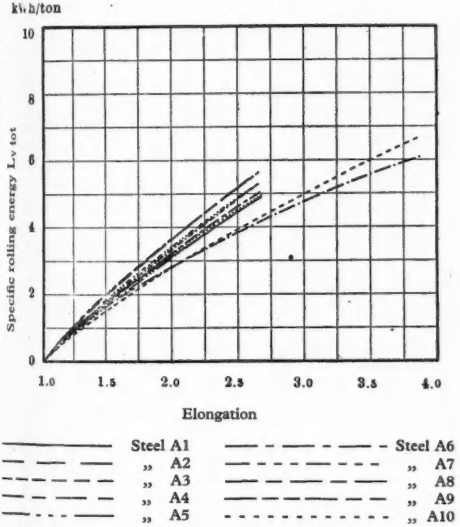

Fig. 3. **Specific rolling energy versus elongation produced in mill A I with the use of open box passes.**

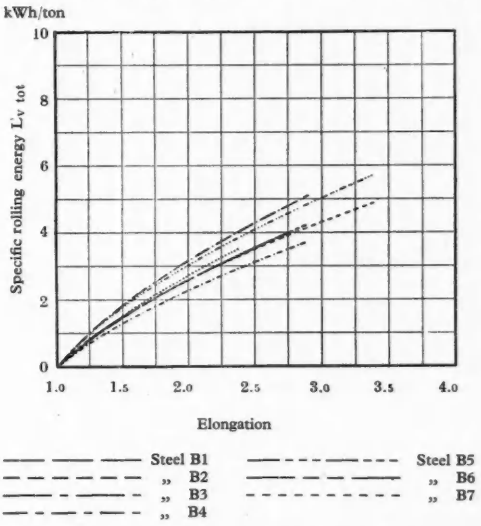

Fig. 5. **Specific rolling energy versus elongation produced in mill B I in open box passes.**

TABLE 2.

Steel	Ingot		Composition of steel, %								
No.	Size, mm.	Weight, kg.	C	Si	Mn	P	S	Cr	Ni	Mo	Cu
B1	305 × 305	675	0.15	0.01	0.11	0.021	0.014	—	—	—	—
B2	330 × 330	953	0.30	0.13	0.54	0.020	0.019	0.09	—	—	—
B3	280 × 280	610	0.65	0.25	0.70	0.021	0.013	—	—	0.22	—
B4	280 × 280	595	1.35	0.19	0.32	0.021	0.011	—	—	—	—
B5	330 × 330	972	1.12	0.28	0.29	0.023	0.014	0.42	—	—	—
B6	330 × 330	768	1.02	0.27	0.30	0.021	0.014	1.63	—	—	—
B7	280 × 280	510	0.08	0.45	0.36	0.019	0.014	17.80	8.30	0.10	—

TABLE 3.

Steel	Ingot		Composition of steel, %						
No.	Size, mm.	Weight, kg.	C	Si	Mn	P	S	Cr	Ni
C1	325 × 325	492	0.11	—	0.38	0.016	0.016	—	—
C2	325 × 325	517	0.49	0.07	0.27	0.029	0.005	—	—
C3	325 × 325	513	1.13	0.24	0.37	0.020	0.012	—	—
C4	325 × 325	516	1.33	0.15	0.26	0.022	0.013	0.35	—
C5	325 × 325	519	1.00	0.32	0.33	0.020	0.012	1.49	—
C6	325 × 325	511	0.09	0.46	0.40	0.018	0.014	18.80	8.80

mill train with flywheel and is driven by a three-phase induction motor through a rope-drive. The four stands are equipped with babbitted roll bearings. The rope drive consists of 18 ropes of 50 mm. dia. each, the reduction ratio being 1 : 3.65. The flywheel of 80 tons weight has a flywheel effect of 3,800,000 kg m², which corresponds to a stored energy of 24,000 h.p. sec.

The rolls of the first stand were made of a 0.7 C, 0.5 Cr steel and had a slight ragging. The materials rolled are shown in Table 3.

The test results were utilised for the establishment of the spec. rolling energy *vs.* elongation diagram shown in Fig. 6.

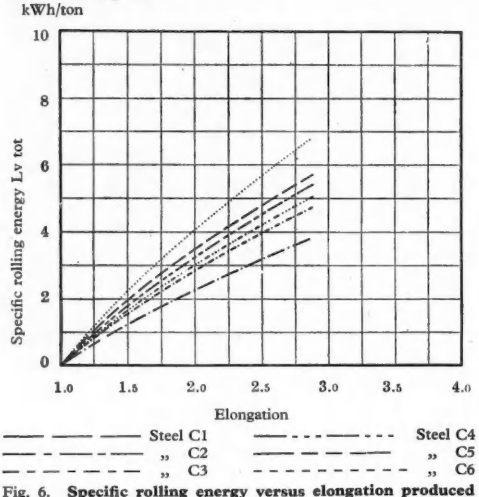

Fig. 6. **Specific rolling energy versus elongation produced in mill C I with open box passes.**

The conclusions drawn from the tests conducted with the aforementioned three mills are as follows :

(a) The specific rolling energy L_v (kg/cm³) per pass increases with increasing elongation as well as with falling rolling temperature.

(b) The mean specific rolling energy $L_{v\,med}$ for a number of passes remains quite constant, although to a certain extent it tends to decrease with increasing elongation.

(c) Both the quality of the steel and—to a still higher degree—the temperature of the ingot and also the uniformity of this temperature throughout the ingot have an extraordinary effect upon the rolling energy required. The greatest energy consumption was registered with the stainless Cr–Ni steel; while at temperatures of 1100 deg. C. and slightly less, the carbon steels on the whole required identical rolling energy irrespective of the carbon content.

(d) The rolling energy requirements of the two-high mill equipped with roller bearings amount to some 75 per cent of a comparative mill equipped with babbitted bearings and to some 85 per cent of the energy requirements of a three-high mill. These figures vary with the temperature of the rolled piece and with the uniformity of its temperature.

(e) In the case of blooming mills with box passes and equipped with roller bearings, the specific energy consumption must be expected to range from 9 to 12 kg m/mm³ for carbon steel and from 10 to 15 kgm/cm³ for alloy steel. Actual values of the energy consumption will depend upon the composition of the material, its temperature and upon the temperature distribution throughout the material. In the case of mills equipped with other types of bearings such as babbitted or synthetic resin bearings, the specific energy consumption will be higher, according to the type of bearings used. Where accurate figures are required, it is necessary to take into account the influence of such factors as steel composition, rolling temperature, roll diameter, roll condition.

Gothic and Diamond Passes.—In order to investigate the energy consumption in mills equipped with diamond passes, the second stand of the aforementioned mill AI was equipped with another set of rolls of forged 0.85 C steel, the roll passes being shown in Fig. 7. The various steels were rolled with identical reductions. The specific rolling energy L_{vtot} in KW hours per ton as it was found with the different steels AI–A10 as function of the elongation, is charted in Fig. 8.

The corresponding data obtained with mill BI with the use of gothic passes are plotted in Fig. 9, where it will be noted that this test comprised the rolling of the same steels BI to B& as used in the original tests. For the purpose of the test, the rolls of the second stand of mill CI were exchanged for rolls with diamond passes. As in the box-pass tests, the steels CI to C6 were rolled. The specific energy consumptions evaluated are charted in Fig. 10.

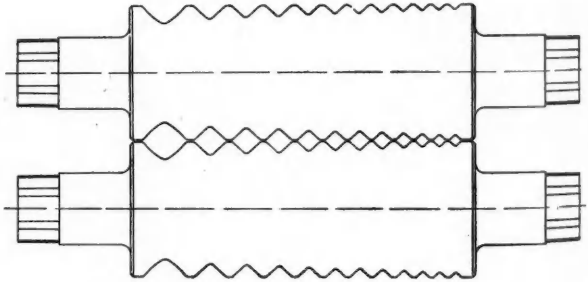

Fig. 7. **Rolls with gothic and diamond passes used with mill A I.**

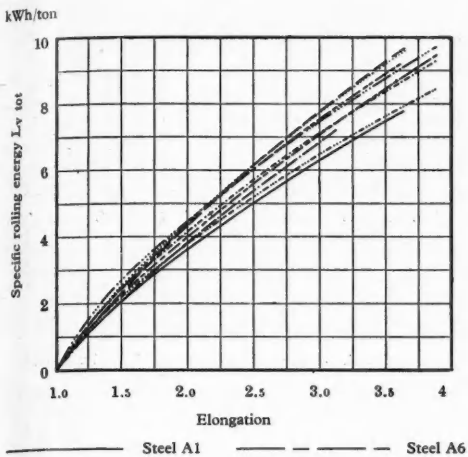

Fig. 8. **Specific rolling energy versus elongation produced in mill A I equipped with diamond passes.**

Similar investigations were conducted on four other mills. The conclusions drawn from these tests conducted with gothic and diamond passes are as follows:

(1) The specific rolling energy L_v(kgm/cm³) rises with increasing elongation and decreasing rolling temperature.

(2) The specific rolling energy required with gothic and diamond passes is some 25-35 per cent higher than that recorded with open-box passes.

(3) The mean specific rolling energy of a series of passes is relatively constant and as in the case of the open box passes, it tends to decrease with increasing elongation, particularly in the case of small passes.

(4) As in the case of the open box passes, the temperature of the piece and its uniformity of temperature are of influence upon the rolling energy required. Again, the stainless Cr–Ni steel requires the greatest rolling energy, while in the case of the plain carbon and of the low alloyed steels the rolling energy requirements are determined by the temperature and temperature uniformity rather than by the composition of the steel.

(5) The power requirements of a two-high blooming mill equipped with roller bearings are some 80 per cent of those registered with a corresponding mill equipped with babbitted bearings, and about 60 per cent of those obtaining with a three-highmill with babbitted bearings. These figures differ considerably from those previously given for rolling in box passes. This shows that in addition to the resistance to deformation there exist some other factors which exert considerable influence upon rolling energy requirements.

(6) In the computation of the power required for the rolling of carbon steel in the gothic and diamond

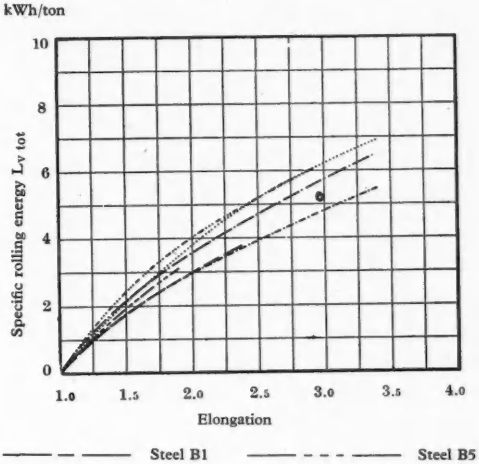

Fig. 9. **Specific rolling energy versus elongation produced by mill B I equipped with gothic passes.**

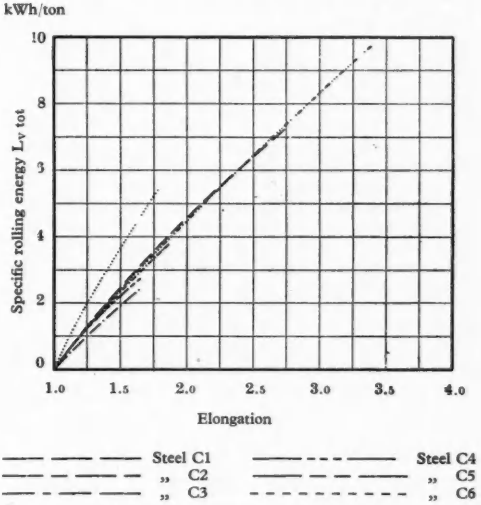

Fig. 10. **Specific rolling energy versus elongation produced by mill C I equipped with diamond.**

passes of blooming, billet, or semi-finishing-mills equipped with roller bearings, the specific rolling energy required must be assessed as $L_{v\,med}$ = 12 to 15 kg/cm³; while a figure of 11–17 kg/cm³ must be taken in the case of alloyed steels. The actual values in a given case will depend upon the alloy-content and the rolling temperature of the material concerned.

COMPARISON OF SURFACE ROUGHNESS OF HIGHLY FINISHED PLANE SURFACES.

By J. KLUGE and G. BOCHMANN. (From *VDI Zeitschrift*, Vol. 88, April 1st, 1944, pp. 179-181).

IN their investigations into problems of lubrication the authors make use of plane sliding surfaces produced by a special lapping process. These surfaces have a smooth velvety appearance free from machining scratches, and they resemble a surface produced by sandblasting. Actually, the surfaces are covered with uniformly distributed surface irregularities.

The roughness of surfaces of this kind is difficult to determine with the use of conventional surface testers as the surface irregularities may approximate to one micron and less in height. Moreover, the irregularities are too densely distributed to permit the employment of the tracer method as the radius of the tip of the tracer point can hardly be made smaller than 10 microns. Nor can the micro-interferometer method be employed, as highly finished surfaces of this kind do not produce any interference bands. Another consideration calling for a new type of instrument was that unskilled helpers should be able to carry out surface measurements rapidly and reliably.

In research work connected with problems of lubrication it is less important to determine the surface profile than to ascertain whether repeated re-finishing of a surface will produce identical surface roughness. For this purpose a new apparatus was developed which, for some time past, has been used with success.

It was considered that an instrument measuring surface reflectivity would serve the purpose. This type of instrument operates on the principle of throwing a parallel beam of light upon the surface under an angle of 45 deg. The reflected beam is then passed through a lens followed by an aperture and a photocell. The electric current produced by the stream of reflected light is measured by means of a galvanometer, the current intensity serving as a measure of the surface roughness. It was found, however, that with an angle of incidence of 45 deg. the usefulness of this type of instrument is limited to the investigation of shiny surfaces, since in the case of dull surfaces its sensitivity and resolving power for different degrees of roughness are too small. It was therefore found necessary to ascertain the influence of the angle of incidence upon the reflectivity of highly finished surfaces having different degrees of roughness. For this purpose a special instrument was built, Fig. 1, which permits variation of the angle of incidence within a range of approx. 20 deg. to 90 deg. Referring to Fig. 1 the slidable tube (b) contains the optical system consisting of a low voltage electric bulb, a condenser, a slit, and a lens, whilst the slidable tube (c) contains a barrier type selenium cell. The cell current is measured by means of a galvanometer having a measuring range of 4.5 micro-amp.

This apparatus was used to investigate nine cast iron surfaces of different degrees of roughness, typical microphotographs of these surfaces being shown in

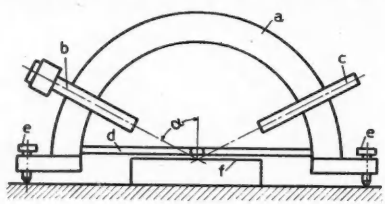

Fig. 1. **Experimental reflecting measuring instrument.** (a) Guide ring (b) illuminating tube (c) barrier cell tube (d) reference level (e) micrometer screws (f) surface of sample (α) angle of incidence

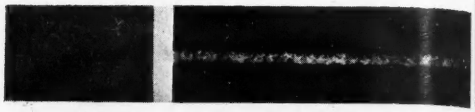

Figs. 2 and 2a. **Surface No. 1, Height of profile abt. 1.1μ**

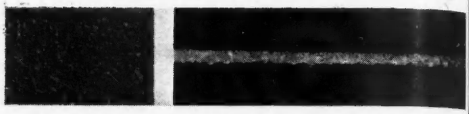

Figs. 3 and 3a. **Surface No. 3, Height of profile abt. 2.4μ**

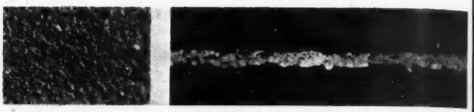

Figs. 4 and 4a. **Surface No. 7, Height of profile abt. 5.1μ**

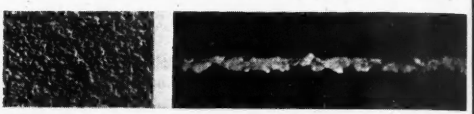

Figs. 5 and 5a. **Surface No. 9, Height of profile abt. 8.7μ**

Figs. 6 and 6a. **Surface No. 5, Height of profile abt. 0.7μ**

Figs. 2-6. These surfaces were also examined with a surface tester according to Schmaltz. The records obtained by this method are indicated in Figs. 2a-6a. As will be seen from these illustrations, surface measurement by means of the light cross-section method according to Schmaltz is rather unsatisfactory, since machining scratches and small cracks remain invisible except in Figs. 2 and 2a, referring to the surface of smallest surface irregularity. Surface irregularities are of course also shown in the case of surface, Figs. 6 and 6a, which is finished by uni-directional polishing. In any event, the particular surface conditions of the surfaces investigated make it difficult to ascertain the height of the surface irregularities with any degree of certainty, and even average values obtained from a number of measurements are rather uncertain.

In order to ascertain the most favourable angle of incidence, the cell current was measured with different angles of incidence and different degrees of surface roughness. The results of these tests are charted in Fig. 7, which shows that in the case of the dull surfaces investigated, angles of incidence smaller than 84 deg. prove unsatisfactory. In Fig. 8 these results are charted as function of the total profile height values, obtained with the light cross-section method according to Schmaltz. All these curves are seen to be hyperbolic. These results indicate that the reflectivity method can be applied to the comparative surface determination of highest quality surfaces if the angle of incidence is chosen according to the required resolving power. But the applicability of this method must remain restricted to

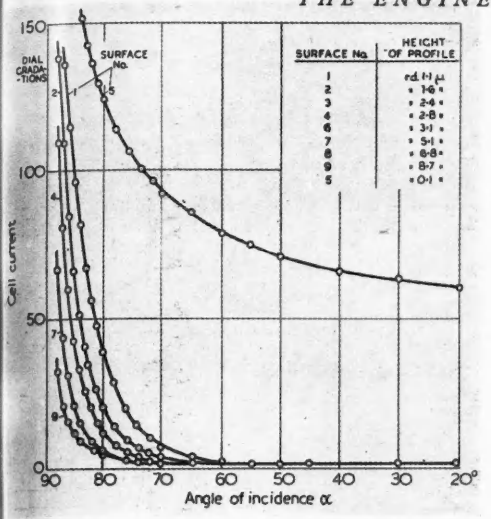

Fig. 7. **Cell current registered with experimental instrument (Fig. 1), as function of angle of incidence for different surfaces.**

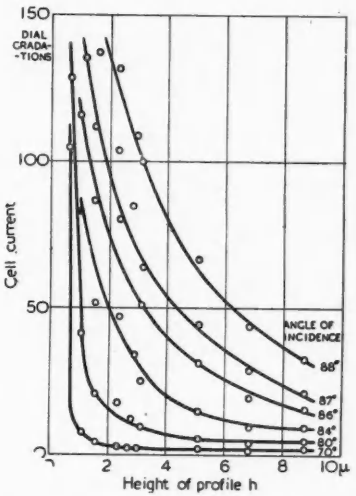

Fig. 8. **Cell current of experimental instrument (Fig. 1) as function of profile height (according to Schmaltz) for a different angle of incidence.**

the comparison of surfaces produced by identical methods.

Taking advantage of these preliminary experiences, a simplified instrument was built which permits the investigation of surfaces with different degrees of surface roughness but produced in identical manner (Fig. 9). As the use of this instrument is to be limited to comparative tests, the degree of surface roughness can be based on any convenient system of roughness units. In order to enable the examination of dull surfaces of highest surface quality with roughness ranging from one to 8 microns, the new instrument has an angle of incidence of 86 deg. This yields a resolving power which is sufficiently high to determine roughnesses ranging from one to 5 microns. The measuring range of the galvanometer does, however, allow roughnesses of one micron to be determined with full accuracy. Both the illuminating device and the cell holder are rigidly set at the aforementioned angularity.

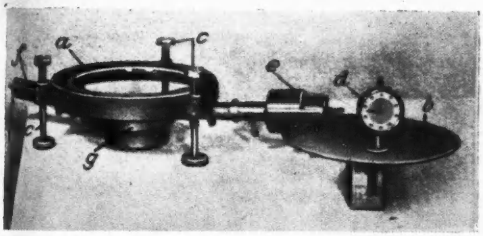

Fig. 9. **Final instrument.**
(a) annular bore (b) cover with dial gauge (c) micrometer screws (d) dial gauge (e) illuminator tube (f) cell tube (g) sample.

Provision is made to prevent the access of extraneous light to the surface under examination. This is achieved by extending the annular base (a) of the instrument as far downward as possible, and by providing a rotatable cover (b) which can be easily taken off. Owing to the annular shape of the instrument, surfaces of up to 150 mm. in diameter can be examined. The level of the examined surface is adjusted to its proper height by means of the three micrometer-screw feet (c). A measuring gauge (d) of the dial type, affixed to the cover of the instrument, is also provided. The elevation of the surface is so adjusted that the reflected beam of light falls upon the centre of the barrier cell. The light intensity can be adjusted by narrowing or widening the slit. This makes it possible to adjust the sensitivity of the instrument to suit requirements.

LUMINOUS INTENSITY OF ARC-LAMP REFLECTORS.

By M. GODFERT. (From *Bulletin de la Societe Francaise des Electriciens*, Vol. 4, No. 37, May, 1944, pp. 125-130)

THE method of calculation given below applies to parabolic reflectors which have a positive arc crater as their source of light. The spherical non-symmetrical arc is approximated by a symmetrical source of light in the focal plane, and the light in a given direction, determined by the angle ϵ with the axis, emanates from different regions of the crater. If these regions are found, the apparent brightness of different mirror points can be determined and the luminous intensity in the given direction evaluated.

It is convenient to imagine the direction of light inverted and to determine the reflection points of all rays under ϵ on the focal plane which contains the crater. The mirror paraboloid has its origin in O and its axis is OX (Fig. 1).

A point M, of the value x, in plane ZOX is considered. All rays falling on M at ϵ with OX form a conical surface. The reflection of this beam on the focal plane is an ellipse with half-axis a and b and the centre at a distance c from OX.

ω = angle between FM and OX

f = focal distance of the mirror

FM = $f + x$, if ϵ is sufficiently small

$$\cos\omega = \frac{f-x}{f+x} = \frac{b}{a}; \quad a = \frac{(f+x)^2}{f-x}\epsilon;$$
$$b = (f+x)\epsilon; \qquad c = a\epsilon\tan\omega$$

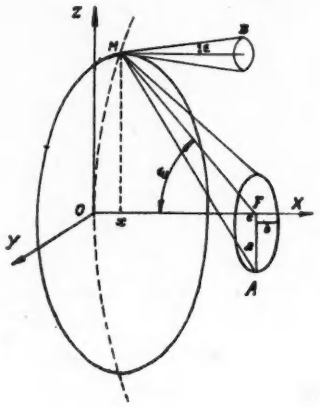

Fig. 1.

The reflection of ray BM in plane ZOX, on the focal plane is A, that is, the end point of the large axis of the ellipse. M′ at angular distance φ from M is now considered (Fig. 2). The beam reflected by M′ on the focal plane is a new ellipse obtained by rotation of the first one by φ.

The reflection of ray B′M′//BM on the focal plane is A″ (Fig. 2) at the angle Ψ from A′.

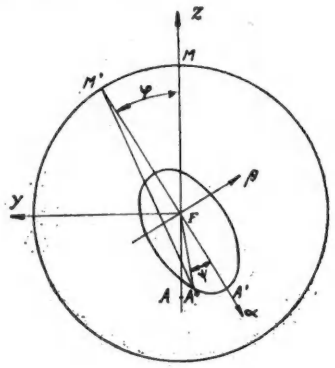

Fig. 2.

$$\tan\psi = \cos\omega\tan\varphi$$

and if ϵ is sufficiently small

$$\tan\psi = \frac{b}{a}\tan\varphi.$$

Calculation of $d = \mathrm{FA}''$:

$$\frac{(\alpha-c)^2}{a^2} + \frac{\beta^2}{b^2} = 1, \text{ and } \beta = \alpha\tan\psi.$$

For A″ it is $\alpha = \alpha_0$; $\beta = \beta_0$

$$\frac{(\alpha_0-c)^2}{a^2} + \frac{\alpha_0^2}{b^2}\tan^2\psi = 1, \text{ or}$$

$$\left(1 + \frac{a^2}{b^2}\tan^2\psi\right)\alpha_0^2 - 2c\alpha_0 - (a^2-c^2) = 0;$$

if ϵ sufficiently small

$$\frac{a}{b} = \frac{1}{\cos\omega} \text{ and } 1 + \frac{a^2}{b^2}\tan^2\psi = 1+\tan^2\varphi = \frac{1}{\cos^2\varphi}$$

and thus: $\dfrac{\alpha_0^2}{\cos^2\varphi} - 2c\alpha_0 - (a^2-c^2) = 0,$

$$\alpha_0 = c\cos^2\varphi \pm a\cos\varphi\sqrt{1-\frac{c^2}{a^2}\sin^2\varphi}.$$

The plus sign applies here

$$d = \mathrm{FA}'' = \frac{\alpha_0}{\cos\psi},$$

$$d = a\frac{\cos\varphi}{\cos\psi}\left[\frac{c}{a}\cos\varphi + \sqrt{1-\left(\frac{c}{a}\sin\varphi\right)^2}\right].$$

If M′ describes a complete circle, A″ describes a closed curve; the co-ordinates of its points are

$$y = -d\sin(\varphi-\psi) \text{ and } z = -d\cos(\varphi-\psi)$$

or

$$y = -\left[\frac{c}{a}\cos\varphi + \sqrt{1-\left(\frac{c}{a}\sin\varphi\right)^2}\right]\frac{a-b}{2}\sin 2\varphi,$$

$$z = -\left[\frac{c}{a}\cos\varphi + \sqrt{1-\left(\frac{c}{a}\sin\varphi\right)^2}\right]\left[\frac{a+b}{2} + \frac{a-b}{2}\cos 2\varphi\right]$$

As $\dfrac{c}{a}$ is very small, the bracket common to both expressions is approximately 1 and the curve described by A″ is very near to a circle. The radius of this circle is $\dfrac{a-b}{2}$ and its centre at the distance $\dfrac{a+b}{2}$ from F. To an angular displacement of M′ by φ, corresponds to a displacement of A″ by 2φ.

If $-\dfrac{c}{a}$ increases, the curve described by A″ changes in form as exemplified by Fig. 3.

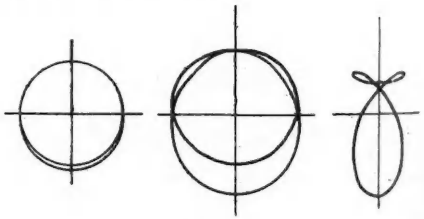

Fig. 3.

The brightness of any point in the crater is a function of d. To evaluate d, the curve described by A″ can be sufficiently approximated by a circle, it will then be

$$d = a\frac{\cos\varphi}{\cos\psi} = \sqrt{\frac{a^2+b^2\tan^2\varphi}{1+\tan^2\varphi}}, \quad \tan\varphi = \sqrt{\frac{a^2-d^2}{d^2-b^2}};$$

This last formula permits, for any of d, i.e., brightness B, to fix the four points of the parallel which have the brightness B.

It is convenient to introduce f as a measuring unit.

We make $x' = \frac{x}{f}$ and $d' = \frac{d}{f}$ thus obtaining

$$\tan\varphi = \sqrt{\frac{\frac{(1+x')^4}{(1-x')^2} - \left(\frac{d'}{\epsilon}\right)^2}{\left(\frac{d'}{\epsilon}\right)^2 - (1+x')^2}}$$

By joining all points of the same value $\frac{d'}{\epsilon}$ on different parallels, a curve of equal brightness is obtained. Indeed for a given ϵ and f it is $d = \epsilon f\left(\frac{d'}{\epsilon}\right)$, which corresponds to a given brightness B.

By varying the values of x' from 0 to 0.5 and $\frac{d'}{\epsilon}$ from 1 to 4, a family of curves is obtained, which embraces all possible cases.

The form of the curves of equal brightness is independent of the size of the mirror, but for a given mirror these are limited by its edge; the curve beam is limited by a circle $R' = \frac{R}{f}$, R = radius of the mirror.

A family of curves of equal brightness and some circles R′ are represented in Fig. 4.

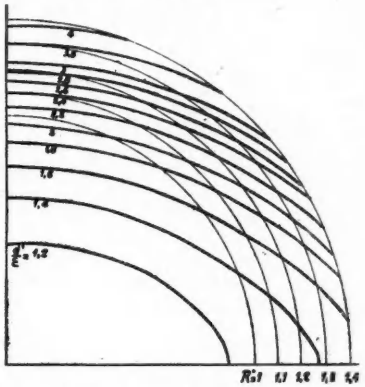

Fig. 4.

The luminous intensity emitted in a direction defined by ϵ, by the surface d between two infinitely close lines of equal brightness is $di = B.\cos.\epsilon.ds$ (where $ds.\cos.\epsilon$ is the surface projected on plane $\perp \epsilon$). For the total surface of the mirror it is

$$I = \int_0^S B\cos\epsilon\, ds$$

S is the total mirror surface projected upon a plane $\perp$ OX. It can always be assumed that $\cos\epsilon = 1$. A new family of curves (Fig. 5) represents $s' = \frac{s}{f^2}$ as a function of

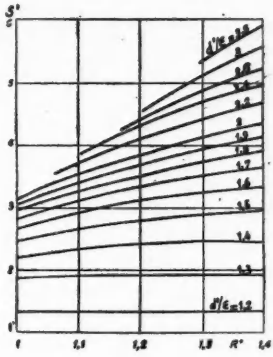

Fig. 5.

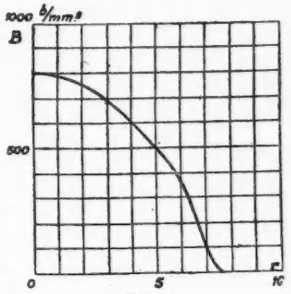

Fig. 6

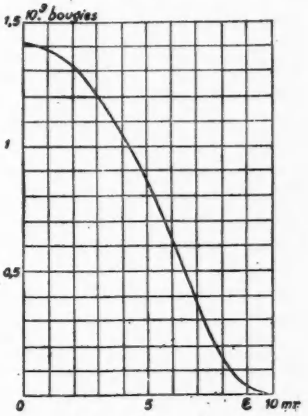

Fig. 7.

R′ for all curves of equal brightness. From these curves it is possible to determine the curve B as a function of s for all values of ϵ; the area between this curve and its axis is $\int B.\,ds$, i.e., the luminous intensity in the considered direction.

Evaluation of the luminous intensity (flux) in a given direction: B as a function of d (B = f (d)) is drawn (Fig. 6). A value of $\frac{d'}{\epsilon}$ is chosen; for d = crater radius ($B = 0$), $\frac{d'}{\epsilon}$ determines ϵ; for this ϵ the brightness $B = 0$. For the same value of ϵ, $d = f\epsilon\left(\frac{d'}{\epsilon}\right)$ i.e., B, should be determined for the lines within the line corresponding to $B = 0$.

By using the family of curves represented in Fig. 5, curves $B = f(s)$ for several values of ϵ can be drawn. Integration of these curves by a planimeter yields the different values of M. These values should be corrected by the mirror efficiency η. Fig. 7 gives the characteristic obtained for a reflector $\phi = 1500$ mm. $f = 750$ mm., the characteristic of the crater used is given in Fig. 6.

The families of curves represented in Fig. 4 and Fig. 5 are independent of the mirror and crater employed and the angles ϵ considered; knowledge of f, B = f (d) of the crater and the angle ϵ permits the evaluation of the values of B for all curves. In direction of the axis, $\epsilon = 0$, all curves have the same value of brightness which is that of the central region of the crater.

INDUSTRIAL DUST SEPARATION AND ITS PHYSICAL PRINCIPLES

By O. SCHÄRER. (From *Schweizerische Bauzeitung*, Vol. 124, No. 5, July 29, 1944, pp. 53-59).

A SPHERICAL dust particle moving through air with a velocity w, is subject to a frictional air resistance which, according to Stokes, is expressed by $K = 6 \cdot \pi \cdot \mu \cdot a \cdot w$, where a is the radius of the particle and μ is the coefficient of viscosity. If a mechanical force, such as the gravitational force G or corresponding force inertia (produced in a cyclone), acts upon the particle, the terminal velocity will be given by

$$w = \frac{2\,(\rho - \rho_0) \cdot g}{9 \quad \mu} \cdot a^2,$$

where g is the gravitational constant (981 cm/sec.^{2}), ρ is the density of the material of the particle, and ρ_0 that of the air. Since G will decrease with a^3, w will decrease in proportion with a^2. A mechanical dust separator therefore operates selectively, effecting the separation of larger particles more efficiently than that of the smaller ones. Stoke's equation is valid for a range of particle sizes extending from 1 micron to approximately 40–60 microns, according to the density of the material. Particles larger than 60 microns will have a terminal velocity which is somewhat smaller than indicated by Stoke's formula, as the latter does not take into account the effect of hydrodynamic inertia.

An empirical formula based upon the experimentally established relationship between Re and K was evolved by Frossling.* Still another relationship was established by Widell † on the basis of modern hydrodynamic concepts. His formula reads $K = c \cdot 4 \cdot \pi \cdot a^2 \frac{\gamma_0 w^2}{2g} = \phi\, d^2 \frac{\gamma_0\, w^2}{g}$, where $d = 2a$, is the diameter of the particle and γ_0 is the specific gravity of the air. The coefficient ϕ is known to be a function of the Reynolds number $Re = \frac{w\,d}{\nu}$, where ν is the kinetic viscosity. According to Stokes, it would be $\phi = \frac{3\pi}{Re}$ if $Re < 1$. For values of $Re < 400$, it is, according to Widell,

$$\phi = \frac{3\pi}{Re}\ (1 + 0.13\ Re^{0.1}).$$

Particles less than 1 micron in diameter have a terminal velocity in excess of that indicated by Stokes' relationship. This is due to the fact that the molecular structure of the air causes a certain surface slip to take place. This phenomenon was neglected by Stokes, who assumed that no slip occurs in the boundary layer of air. However, Stokes' expression is sufficiently accurate for practical purposes.

A simplified formula established by Cunningham reads as follows :

$$\frac{w}{K} = \frac{1}{6\,\pi\,\mu\,a} \left(1 + A\,\frac{l}{a} \right)$$

where $l = 0.06$ microns is the free length of the path of travel of the air molecules at 0 deg. C. and 760 mm. barometric pressure, and $A = 0.87$ is a constant.

Mechanical separation suffers from the disadvantage that the separating mechanical force decreases with the square of the diameter of the particle. In the range of small particle sizes more favourable conditions are offered by the principle of electrostatic precipitation. In this case the separating force is equal to $E \times Q$, where E is the strength of the field and Q is the electric charge of the particle. As Q varies with a^2, the terminal velocity w is in linear proportion with a. With electrostatic precipitation the separating force acting upon a particle of 1 micron diameter will, therefore, be one-tenth of that applied to a particle of 10 microns, but in the case of mechanical separation by centrifugal force the 1 micron particle will receive only one-hundredth of the separating force acting upon the 10 micron particle. Where dust of great fineness is involved, such as, for instance, dust of 5 micron particle size, electroprecipitation is, therefore, theoretically superior to the mechanical method. Furthermore, in the case of particles of less than 1 micron the electric charge Q varies in straight proportionality with a, so that w becomes altogether independent of a, which lends additional superiority to the electrical method.

For the purpose of electroprecipitation, an electric charge must be imparted to the particles to be removed from the gas stream. This is effected by ionisation of the carrier air or gas which leads to the deposition of ions upon the dust particles. Once the electric charge has been imparted, the particle is driven to the collecting electrode by the force of the electric field E.

The diagrammatic view of a pipe-type electroprecipitator is given in Fig. 1. Here the centrally located wire electrode of the radius ν is raised to a high negative potential, while the surrounding pipe of the radius R which serves as the collecting electrode is connected to earth. In Fig. 1 the dust laden air is assumed to flow through the pipe in an upward direction with a velocity v which is so chosen that laminar flow would exist if no corona effect were present to cause turbulent motion of the air.

The electrical phenomena which take place in an assembly of this kind will be governed by the strength of the electric field E_r at the wire and E_R at the cylinder inside wall. In the computation of the strength of the field E the following three cases must be considered, viz :—

E if no corona discharge occurs, that is, if the field is a purely electrostatic one with the current i = O and with no dust being contained in the air.

E^1 if corona discharge takes place resulting in i > O, but with no dust being carried by the air.

E^{11} if corona discharge prevails and the air is laden with dust, the current intensity being $i'' > O$.

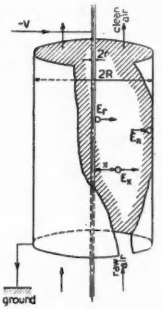

Fig. 1. **Diagrammatic view of pipe type electroprecipitator.**

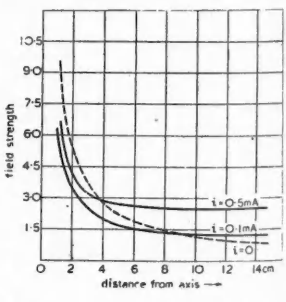

Fig. 2. **Strength of electric field in pipe electrode.**

If an increasing potential V is applied to the wire, the field strength will increase in linear proportionality with V until a limit value of $E_r°$ is reached. At this limit, which is given by $E_r° = 33.9 \cdot \rho_o + 10\sqrt{\frac{\rho_o}{\nu}}$ corresponding to a voltage V°, the field strength is stabilised, any further increase in V leading to a corona discharge producing a current i. This current then increases with the second power of V. If the air is laden with dust, the value for V° is increased in approximate proportion with the additional space charge introduced by the dust.

Referring to Fig. 2, E is seen to decrease with increasing distance from the wire and reaches a value of $E_R = \frac{V}{R} \frac{1}{\ln R/r}$ at the internal wall surface of the pipe electrode. The corona field E^1_r at the cylinder, however, is no longer a function of R, but is related to the current i by the relationship $E^1_R = \sqrt{\frac{2i}{u}}$ where u is the specific mobility of the negative ions of the air, which has a numerical value of 1.75 cm. per second per V per cm. The variation in E^1_R with the distance from the wire electrode is charted in Fig. 2. If the air is laden with dust, a somewhat different characteristic is obtained which is also charted in Fig. 2. Here E^{11}_R is seen to be larger than E^1_R, which means that in the presence of dust, the potential difference between the electrodes is increased. Or, in other words, the dust tends to suppress the corona discharge. For this case the following approximate relationship has been established by Pauthenier, to wit :—$E^{11}_R = E^1_R \left(1 + \frac{p \cdot S \cdot R}{3}\right)$ where S is the total surface of the dust in cm.² and p is a factor of polarisation related to the dielectric constant of the dust by the expression $\rho = 1 + 2\frac{\epsilon - 1}{\epsilon + 2}$. Vice versa, if the voltage is maintained constant, the presence of dust will lead to a decrease in the current from i to i^{11} according to the expression $\frac{i^{11}}{i} = 1 - \frac{p \cdot S \cdot R}{3}$.

Pipe-type electroprecipitators are only rarely employed in modern practice, and in most cases parallel plates are employed with the wire electrodes placed between the plates. Correct proportioning of the distances between adjacent wires is important, since an unduly small distance interferes with the development of the corona discharge; while an excessively large distance between the wires results in a deficiency in corona discharge.

The efficiency of electroprecipitation is defined by

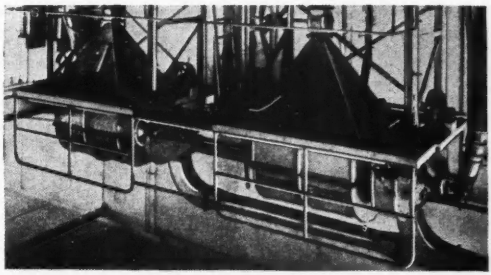

Fig. 3. **Elex-Jaffhor dust collector plant.**

the expression $\eta = \frac{n_a - n_e}{n_a} = 1 - e^{\frac{-2 \cdot w_R \cdot l}{R \cdot v}}$ where l is the length of the precipitator from the point of raw air admission to that of clean air discharge, n_a is the initial dust concentration and n_e is the final dust concentration of the air or gas passed through the precipitator.

A large precipitator plant for the treatment of waste gases discharged by the electrolytic furnaces for the production of aluminium is installed at the works of the Aluminium Industries Ltd. at Chippis, Switzerland. Waste gases of this kind contain obnoxious constituents such as fluor and sulphurous acid in addition to solid fluorides, soot, and tar vapours. Before admitting these gases to the precipitator, they must, therefore, be subjected to a combined cooling and chemical process, which is effected by injection into the gas of a soda solution in the form of a finely divided spray. The solid dust and the tar are then precipitated in a dry-type precipitator, while the residual amounts of fluor, sulphur, and tar are removed in a wet-type precipitator.

Compared to cyclones of the stationary type, the rotary drum type separator possesses a number of advantages, such as the possibility of adjusting the speed of the rotary drum in accordance with the fineness of the dust and the quantity of air to be dealt with. This type of separator is exemplified by the Elex-Jaffhor dust collector, a twin-installation of which is shown in Fig. 3. Separators of this type are said to give highly satisfactory service in flour mill plants where a very fine and light variety of dust must be dealt with. A modified design known as the Elex Rotor is claimed to secure the efficient separation of coal dust. A disadvantage of this type of separator is that its pressure drop requirements are as great as those of the stationary cyclone. Also the incorporation of rotating parts results in greater cost of maintenance. On the other hand, the efficiency of the rotary type is less affected by partial load and by moisture. In plants dealing with foundry dust, optimum efficiency can be achieved by the injection of steam or atomised water.

*Gerlands *Beitrage zur Geophysik*, 51, 1937, p. 167.
†*Zeitschr. VDI*, 80, 1936, p. 1497.

TESTING NON-FERROUS METALS BY NEW MAGNETO-INDUCTIVE METHOD

By W. SCHIRP, V.D.E., Berlin. (From *Elektrotechnische Zeitschrift*, Vol. 64, No. 31/32, August 12th, 1943, pp. 413-415).

THE magneto-inductive method is particularly suitable for obtaining series measurements on pipes, bars, profiles, pressed parts and sheets of non-ferrous metals, as it allows the detection, in a single operation, of defects in the material (cracks, funnels, porosity, scaly surface, enclosures of foreign materials), of variations in the properties of the material due to the heat treatment (hardness), of changes in the composition (of alloys), and also of variations in the dimensions (diameter, thickness of tubes). The method is based upon the principle of a conductor passing through one or two solenoid coils, connected to an a.c. source of audible frequency. Eddy currents are induced by the solenoids in the material under test (on a length corresponding approximately to the length of the coil); the intensities of these short-circuit currents vary with the properties and the dimensions of the material which may be considered as the secondary winding of a transformer

where the solenoid coil constitutes the primary. It is obvious that the properties of the " short-circuited secondary winding " influences the impedance of the solenoid which can be measured by any bridge method for a.c. If one branch of the bridge is formed by an exactly similar solenoid pulled over a sound part of the work piece used as a standard, any variation in the properties of the material under test will provoke a potential difference at the terminals of the neutral branch of the bridge. This potential difference, after amplification, may be used to indicate—by optical or acoustical means or directly by marking on the material —any deviation from the properties of the standard. Certain difficulties arise, however, if the testing apparatus is to be used for series measurements in the industry where the following conditions must be fulfilled :

1. Defects as well as variations in dimensions, variations in the heat treatment and in the composition of the material must be measured in one operation and at the highest possible speed (about 1 m/sec.).

2. The high speed rules out any direct reading by the operator on the indicating instruments or on the cathode-ray tube, faults must be marked automatically and directly on the material under test. The sound and the faulty pieces must be sorted out automatically.

3. Marks on faulty pieces must differentiate between local defects (cracks, etc.), variations in the properties of the material (hardness), its composition and dimensions (diameter, thickness), in respect to the standard.

The conditions mentioned under 1, can be easily fulfilled by the use of indicating instruments of low or no inertia, such as cathode-ray tubes, electric eyes, etc. The conditions listed under 2, can be fulfilled only by the use of quick-acting relays responding even to impulses of very short duration (fractions of a milli-second) ; this condition necessitates the use of vacuum-tube amplifiers. The relay actuates a signal lamp, and an ink recorder marks the faulty spot on the material, whilst a sorting apparatus sorts out the faulty and sound parts.

The condition ad. 3, i.e., the differentiation between the indication of local faults, called " fault measurement," from indications of variations of the dimensions and the properties of the material, called " comparative measurement," may be achieved by connecting the coils in two different ways. In the first case both coils are drawn close to one another over the material under test, whereas in the second, one coil is drawn over the material under test and the other coil over a standard piece (Figs. 1a and 1b).

In the case of " fault measurement," as the dimensional and physical properties are the same over the whole length of the material, deviations from the standard values are not registered by the bridge, although local faults, which pass first through one and then through the other coil, disturb the equilibrium of the bridge and bring about two impulses (when passing through the first and when passing through the second coil).

The " comparative measurement " indicates in principle dimensional and physical deviations as well as local faults. The sensitivity of the apparatus necessary for the indication of local faults being well above the sensitivity required for detecting dimensional and physical deviations, it is possible to eliminate the indication of local faults without interfering with the other measurement.

The problem whether an indication obtained by the " comparative measurement " is due to deviations in the composition of the material, to its heat treatment, or to dimensional deviations, is solved by phase angle indication on the cathode-ray tube which forms part of the apparatus.

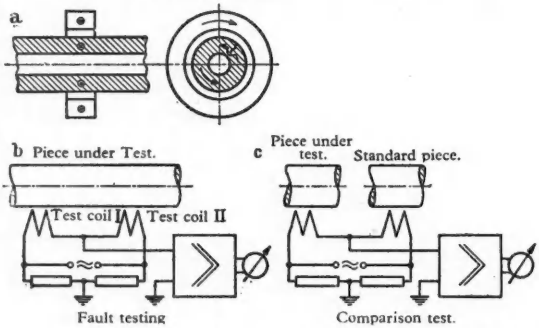

Fig. 1a. **Direction of currents in test coils and material tested.**
Fig. 1b. **Connection diagram for " fault testings " on bars and pipes.**
Fig. 1c. **Connections for " comparative measurement " on bars and pipes.**

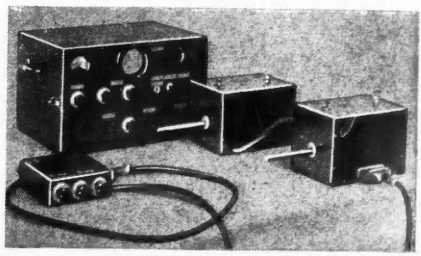

Fig. 2. **Measuring apparatus with selector switch box and testing coil sets for tests on pipes and bars of non-ferrous metals.**

Fig. 2 shows an outside view of the test set described. It consists of the measuring apparatus proper, containing transformer, rectifier, generator for audible frequency a.c., amplifier, relays, indicator ; a selector switch for " comparative " or " fault " measurement, and sets of coils for both measurements. Each set of coils may be used for material with an outer diameter within certain limits, e.g., 8 to 100 mm. in steps, the range of the individual coils being 2.5 to 10 mm. wide. The coils are easily interchangeable. The dimensions of the measuring apparatus are 400 × 250 × 300 mm., its weight about 15 kg. It can be supplied from either 220 V. or 120 V. a.c. mains, and consumes about 120 W.

To enable the full utilization of the high speed limit of the measuring set (1 to 1.5 m/sec.), the material is handled by a motor operated transporter, which, together with the measuring set, forms one unit and as such has been in successful operation for about two years.

Measurements are carried out in the following way :

The bars to be tested are brought up to the set on special "trolleys" (Fig. 3) and slide one by one towards the transporter, where they are caught between motor driven rollers and pushed through the testing coils. At the outset, the selector is in " comparative measurement " position, which means that the " comparative measurement " coils are connected to the amplifier. Thus, the first 200 mm. of the total length of the bar are tested for composition, heat treatment and dimensions. If there is no inacceptable deviation from the standard values the bar is marked by an ink recorder on the first 200 mm. of its length as soon as the bar emerges from the " coil block " (the length of which is 200 mm.). The selector is then automatically switched over for " fault measurement," thereby connecting the corresponding coils to the amplifier and disconnecting the " comparative measurement " coils.

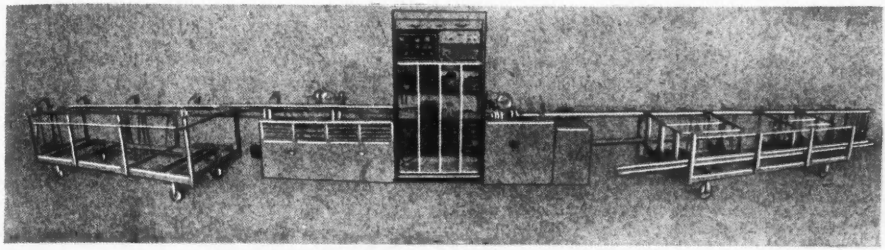

Fig. 3. **Complete testing installation for automatic operation.**

The remaining length of the bar (the total length minus 200 mm.) is then subjected to "fault testing," faults in this case also being marked by an ink recorder directly on the work piece. The feed is 0.6 mm./sec. for the first 200 mm. and, after switching over to "fault testing," 1.5 m/sec. After passing through the testing coils the work is either transported to a trolley (if not faults were recorded) or dropped automatically into a container, if the piece is faulty. The only deficiency in this method lies in the fact that the first 200 mm. of the work is not tested for faults. This may be avoided, however, by the use of two separate sets of measuring apparatus to which the "comparative" and "fault" coils are connected. In this case both tests may be carried out concurrently and over the whole length of the piece.

Testing apparatus of the type described were most successful in detecting very fine longitudinal cracks sometimes invisible on the surface, cracks on the boundaries of areas of different grain, scaly surfaces, and other faults on bars, pipes and other work pieces of light and coloured metals. Though the present method cannot be applied for fault detection in irregularily shaped work pieces (e.g., pressed and forged material and sheet metal), it may be used successfully for testing the heat treatment (hardness) or the composition (alloy) of such materials and special coil-apparatus has been developed for this purpose.

ENGINE, MAN, ANIMAL AND PLANT

By WA. OSTWALD. (From *Schweizerische Bauzeitung*, Vol. 124, No. 3, July 15, 1944, pp. 27-29).

INHALING oxygen and exhaling carbon dioxide, both man and animal have much in common with an engine. Carbon dioxide and water vapour are produced by the combustion of food stuffs or power producing fuels with oxygen. In engines this combustion process is carried out by the production of a flame at high temperatures of the order of 1000 deg. C. and more; while in the animal body a process of invisible combustion takes place at a temperature of 36 deg. C. and less. An engine requires, per horse power hour, from 200 to 400 g of fuel, equivalent to some 2000-4000 kcal; while man, who is able to produce approximately 1 horsepower per day at the rate of one-tenth horsepower for 10 hours, requires the food equivalent of 3000-4000 kcal.

Entirely different from man, animal, or engine, is the plant. On the one hand, the plant sustains its life by burning, at moderate temperature, its own compounds of carbon and hydrogen with the use of atmospheric oxygen, the final products being carbon dioxide and water. But to a much greater extent the plant performs an entirely opposite process by means of its green chlorophyll apparatus. Breathing atmospheric carbon dioxide and drawing water from soil and atmosphere, these constituents are combined by the chlorophyll apparatus into combustible compounds of carbon and hydrogen, starch, cellulose, and fats. The energy required in the performance of this process is derived by the plant from solar radiation. A plant is, therefore, comparable to an engine operating on a reversed cycle, drawing in, as it were, exhaust gases and delivering fuel.

Neither man, animal, nor engine could exist without the co-existence of plants. It is easy enough to visualise a lonely island possessing an abundant vegetation with no animal life. But an island devoid of vegetation and crowded with human and animal life, is not so easily visualised. Indeed, such a population would be doomed to die of starvation once the strong had devoured the weak, since neither human nor animal bodies are equipped with means to utilise solar energy for the sustenance of life. The only way in which such a vegetation-less island could be made habitable by man would be by the exploitation of water, wind, or tidal power for the purpose of producing synthetic food. But this would not be a simple task, nor if achieved could it compare with the astonishing simplicity with which it is carried out by the living organism of the plant.

It is no exaggeration to say that man owes his life to the struggle of the plant against the rotting and rusting of an easily oxidisable world. Indeed, our entire civilisation is characterised by the production of oxidation; our fires oxidise coal, wood, and oil, and oxidation is carried out by our engines and even by our domestic animals. Even where we carry out processes of reduction, such as in the production of iron from ore, we incur the oxidation of a corresponding quantity of other material. Considering the increase in global oxidation brought about by man, it is important not only to practice economy in the exploitation of combustible materials, but to stimulate vegetal growth in a wider sense. Also full use should be made of sources of natural energy, such as water and wind power, which are capable of effecting reduction without involving a corresponding process of oxidation. Certainly the tremendous and still increasing wastage of coal and oil resources stored up in ages past is altogether inexcusable.

No matter whether an internal combustion engine or a plant is concerned, all these processes are based upon the exploitation of the various chemical combinations mutually incurred by three chemical elements, namely, carbon, hydrogen, and oxygen. These processes can be represented graphically in the most informative manner by means of the C–H–O triangle shown in Fig. 1. This diagram comprises the entire range of chemical combinations between C, H, and O that can be envisaged. The corner points of the triangle represent 100 per cent carbon, hydrogen, and oxygen respectively; while points on the three sides of the triangle indicate the entire range of the respective combinations of the two elements represented by the contiguous corner points. Furthermore, any point within the area of the triangle represents a combination between all three elements, their respective percentages, in "atom percent," being determined by the disposition of the point considered.

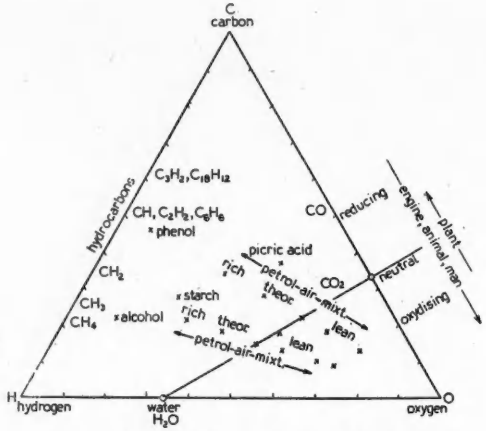

Fig. 1. **The C-H-O diagram of life and death.**

The point midway between the line connecting C and H represents all those compounds which contain equal atom percentages of carbon and hydrogen, such as acetylene (C_2H_2) and benzole (C_6H_6). Nearer point C are found the hydrocarbons, such as naphtalene (C_8H_{10}) and anthrazene ($C_{14}H_{10}$); while compounds richer in hydrogen, such as methane (CH_4) are represented by points nearer point H. Along the lines connecting H with O and C with O respectively, only a very few compounds exist. As a rule H and O combine to H_20 (with 67 atom per cent H). The less common compound H_2O_2 (with 50 atom per cent H) will have its place halfway between points H and O. On the C–O line the halfway point will correspond to CO with 50 atom per cent C; while the distance of the CO_2 point from O will be one-third the distance from C to O. Both the CO_2 and the H_2O point are characterised by the fact that these compounds have no calorific value. Moreover, since this also applies to all mixtures of H_2O and CO_2, a straight line connecting the H_2O and CO_2 points will divide the area of the triangle in two parts, the larger area containing the combustible (oxidisable) substances and the other smaller one containing the burned, thermally degraded, or even oxidising, CHO compounds. On this line lie, in addition to exhaust gases, also those

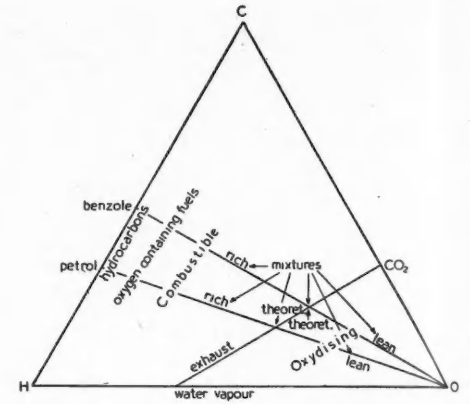

Fig. 2. **Combustion of petrol and benzole in engines.**

compounds and mixtures in which the combustible constituents are complemented by the exact amount of oxygen required for combustion. The theoretical fuel, petrol-air mixture for the Otto cycle, also lies on this line. Lean mixtures will be represented by points located in the small triangular area, while rich mixtures are represented by points lying within the larger, trapezoid area. Near the dividing line, but still within the triangular area lies the point representing nitroglycerine.

A few of the manifold compounds, represented by points within the larger "combustible" area, are exemplified in Fig. 2; while the "oxidising" small triangle must remain empty, since there exists very few well-known oxidising CHO compounds. A straight line drawn from any point representing a hydrocarbon to the oxygen point O will intersect with the CO_2-H_2O line. It is a remarkable fact that these lines intersect in such a manner, that the lengths of the four sections produced serve to indicate the correct composition in atom per cent of the correct fuel-air mixture, and also the CO_2-H_2O composition of the exhaust gases. The entire combustion process is thus expressed, as it were, by a single line; and this applies also to other CHO compounds, such as alcohol or cellulose.

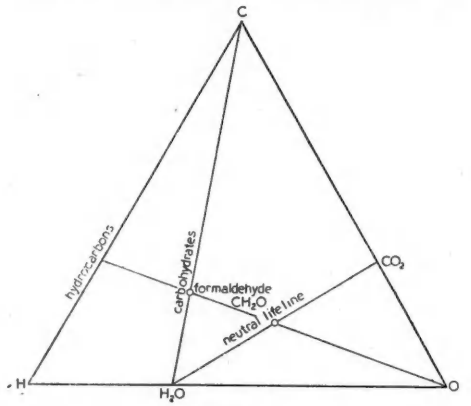

Fig. 3. **The production of carbohydrates by the plant.**

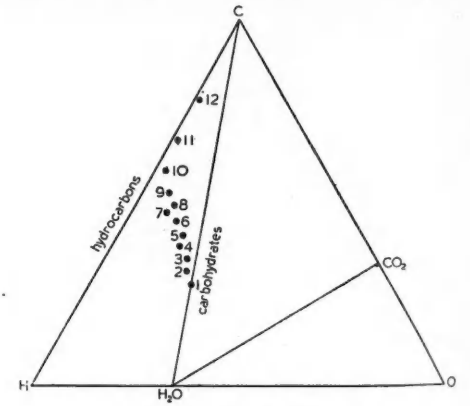

Fig. 4. **The process of carbonisation.**
(1) Cellulose (2) wood (3) wood decomposed (4) peat (5) lignin (6) lignitic brown coal (7) brown coal (8) bituminous coal (9) gas coal (10) coking coal (11) lean coal (12) anthracite.

In addition to yielding information on air requirements and exhaust gas analysis, the CHO triangle affords a profound insight into the process of life in general. The "reducing" area comprises a domain of the organic life of man, animal, and plant; while the "oxidising" triangle includes the activity of the energy-storing chlorophyll apparatus of the plant. The two areas are divided by the CO_2-H_2O "lifeline." Man derives his sustenance from the compounds comprised by the trapezoid and transforms his nutriment together with oxygen into carbon dioxide and water of the neutral line. Vice versa, the plant absorbs water and carbon dioxide and transforms them into the nutriments contained in the trapezoid as well as separating the oxygen.

In Fig. 3 a straight line is drawn from the water point on H-O to point C. All compounds of carbon and water, that is to say, all carbo-hydrates, will be represented by points along this line. Of outstanding importance among these compounds are starch, cellulose, acetic acid, sugar, etc. This line is intersected by the CH_2-O line at the point corresponding to Formaldehyde, which is known to serve as the basis of the assimilating power of the plant. Moreover, the CH_2-O line exactly cuts the neutral "lifeline" in half, this point of intersection corresponding to the compound H_2CO_2, which consists of equal parts of water and carbon dioxide. Furthermore, it is known that the plant releases as much oxygen as it absorbs of carbon dioxide. We, therefore, witness, as it were, the production by the plant of oxygen and carbo-hydrates from equal atom percentages of carbon dioxide and water vapour; and it is not surprising to find that, as the diagram shows, oxygen and carbo-hydrates are produced by the plant in the ratio 2:1.

As evidenced by Fig. 4, the C-H-O triangle also shows the various stages of carbonisation extending from cellulose to anthracite. These stages are seen to be represented by a series of points along a curve of peculiar shape, indicating a process of dehydration finally followed by dehydrogenation.

ECONOMIC CHARACTERISTICS OF THE HIGH SPEED DIESEL ENGINE

(From PROFESSOR T. M. MELKUMOV'S Book, *Theory of the High-Speed Diesel*, Moscow, 1944, pp. 302-311 and 332-340.)

IN order to establish the maximum capacity of the engine, it is necessary to take its design details into account, since these are the decisive factors. In general the fuel/air ratio obtaining at maximum load will not ensure complete and well-timed combustion of the fuel in the cylinder. If the speed of the engine remains unchanged and the load decreases, then the specific fuel consumption must decrease because of the gradual improvement of the combustion conditions. But, as tests have shown, the specific effective consumption upon attaining a minimum C_{emin} as the load is decreased, begins to increase anew (Fig. 1). The effective output at which minimum specific fuel consumption is obtained at a given engine speed is termed the economic output. For different engine speeds different economic outputs of the engine obtain.

When testing a Diesel engine it is found that with falling load at constant engine speed the indicated efficiency increases at first relatively fast and then gradually towards some highest value. In the range of very small loads the indicated efficiency may once more diminish because of the insufficient atomisation of the small fuel quantity and also because of the relatively higher thermal losses to the cylinder walls. The frictional losses change but little with falling load at constant engine speed, particularly if the thermal conditions of the engine remain constant. At constant engine speed the frictional power loss of the idling engine is only a few per cent smaller than that at full engine load. If the Diesel is coupled with a mechanical or hydraulic transmission, the mechanical losses in the transmission also remain practically constant, irrespective of load variations. But at the same time, the indicated output decreases; therefore the mechanical efficiency η_m must droop with falling load. When the engine is idling N_e is zero and $N_i = N_r$ or $N_i = (Nr - \Delta N_r) + N_e$. Thus the mechanical efficiency η_m is nil and $C_e = \infty$. In marine and in stationary practice it is usual to estimate the full load consumption on the basis of the fuel consumption of the idling engine, and the engine showing lowest fuel consumption in idling will prove to be the most economical.

In order to illustrate this point, a graph based on actual test results is given in Fig. 2, the graph having been obtained by the author from a test with an ordinary four-stroke cycle, single cylinder Kolo-VVA Diesel engine. *This chart shows clearly the influence of the various operational factors upon the engine economy with changing load, with the engine speed remaining constant at* 1000 *r.p.m.*

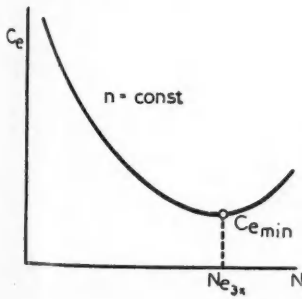

Fig. 1. Variation in Ce with the engine output for constant engine speed.

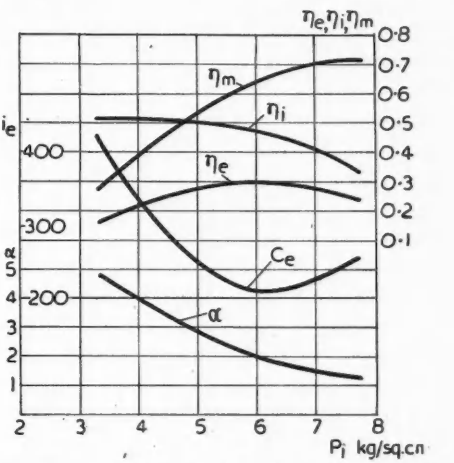

Fig. 2. Characteristics of KOLO-VVA Diesel engine running at 1,000 r.p.m.

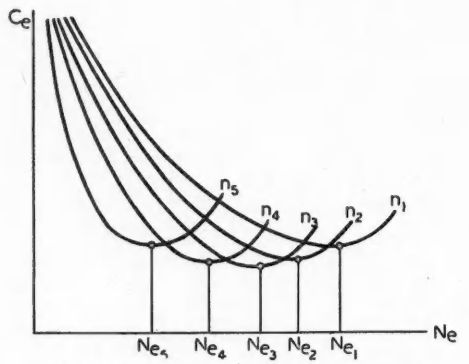

Fig. 3. **Economic output at various engine speeds.**

By making a series of test runs at various constant speed ranges graphs such as that shown in Fig. 3 are obtained which demonstrate the influence of the engine speed upon the economic output. Such results may also be charted on the basis of economic output *versus* engine speed, as shown in Fig. 4, where the minimum specific fuel consumption characteristic as function of the engine speed is given.

There are several ways in which the curves of the economic output and of the minimum specific fuel consumption may be obtained. Thus if the engine is tested by means of a dynamometer or a variable pitch propeller, the respective output and fuel consumption characteristics may be used to determine the load at which minimum fuel consumption occurs. The interrelationship between engine output and specific fuel consumption of a six-cylinder Benz Diesel engine is charted in Fig. 5, which is based on a test conducted by the author.

If the Diesel engine is used to drive a variable pitch propeller with automatic adjustment, the engine speed will be kept constant within certain limits of load variation. The engine characteristic will be analogous therefore to that shown in Fig. 2.

ALTITUDE CHARACTERISTICS OF THE FOUR-STROKE CYCLE DIESEL ENGINE.

The altitude operation of an aviation Diesel engine can be carried out in various ways, two of which are of particular interest. In the first of these, as the weight of air supplied to the cylinder is diminished at higher altitudes, the fuel supply is throttled correspondingly, thus maintaining the fuel/air ratio at its ground level value. In the second method the rate of fuel supply is left substantially unchanged until a certain altitude is reached. The excess air rate is thus decreased because of the smaller density of the air at high altitude. This procedure is feasible in the case of a Diesel engine, since the great excess of air permits some overloading, which becomes less dangerous at increasingly higher altitudes because of the decrease in barometric pressure and air temperature. The altitude up to which the fuel rate may remain unchanged and the maximum permissible value of $\beta = \beta_{max}$ are dependent upon the design of the engine as well as upon the value of β_o at ground level.

Actual flight tests have shown that the second mode of operation can be realised in practice. It is evident that after attaining the altitude which corresponds to $\beta = \beta_{max}$, any further rising of the plane will make it necessary to decrease the fuel rate. The functionality of both the output variation of the engine and of the variation in specific fuel consumption must depend upon the method adopted. In the following the two aforementioned methods will be applied to a Diesel engine not equipped with a supercharger, assuming constant engine speed.

If β remains constant, the indicated efficiency η_{ih} at altitude will equal ground level efficiency η_{io}, and C_{ih} will also be equal to C_{io}. In this case the indicated engine power can be expressed by $N_i = k \cdot \eta_v \gamma_h \cdot n$. The ratio of the indicated engine power at ground level and at altitude respectively will therefore be given by

$$\frac{N_{ih}}{N_{io}} = \frac{\eta_{vh}}{\eta_{vo}} \frac{\gamma_h}{\gamma_o} = \frac{P_h}{P_o} \sqrt{\frac{T_o}{T_h}} = \Delta \quad .. \quad (1)$$

The power loss due to mechanical losses decreases but little with the altitude. Making $N_{rh} = N_{ro} = \text{const.}$ we have $N_{eh} = N_{ih} - N_{rh} = N_{io}\,\Delta - N_{ro}$.

Also $N_{io} = \dfrac{N_{eo}}{\eta_{mo}}$; $N_{ro} = N_{eo}\left(\dfrac{1}{\eta_{mo}} - 1\right)$

Therefore $N_{eh} = N_{eo}\left[\dfrac{\Delta}{\eta_{mo}} - \left(\dfrac{1}{\eta_{mo}} - 1\right)\right]$ (2)

Or by introducing $\dfrac{\Delta}{\eta_{mo}} - \left(\dfrac{1}{\eta_{mo}} - 1\right) = A$ .. (3)

equation (2) becomes $N_{eh} = A_1 N_{eo}$ .. .. (2a)

This expression permits the determination of the decrease in power output with the altitude in the case of an aviation Diesel engine without supercharger, assum-

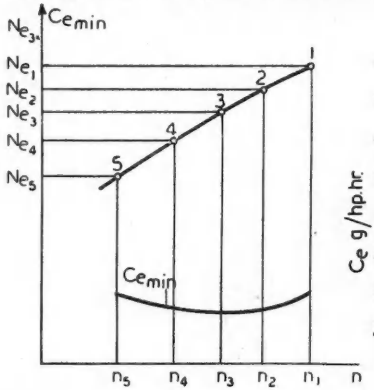

Fig. 4. **Economic characteristics of a Diesel engine.**

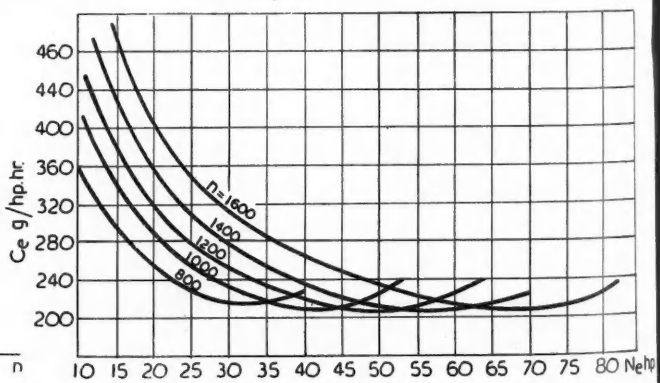

Fig. 5. **Fuel rates of BENZ Diesel engines.**

ing constant values for β and η, while the mechanical efficiency η_{mo} at ground level is also known. For a value of $\eta_{mo} = 0.85$ it is $A_1 = 1.18\Delta - 0.18$ .. (4)

The variation in mechanical efficiency with the altitude can be easily found from the relation

$$\eta_{mh} = \frac{N_{eh}}{N_{ih}} = \frac{A_1 N_{eo}}{N_{io} \cdot \Delta} = \eta_{mo} \frac{A_1}{\Delta} \quad .. \quad (5)$$

and the variation in the fuel consumption per effective output hour can be determined from the equation

$$C_{eh} = C_{eo} \frac{\eta_{mo}}{\eta_{mh}} = C_{eo} \frac{\Delta}{A_1} \quad .. \quad .. \quad (6)$$

A comparison of the results obtained with the corresponding formulae established for Otto engines shows that the decrease in power with the altitude and the increase in the fuel consumption are approximately equal in both cases.

If G_1 = constant and $\beta \neq$ constant, the respective values of β for a given altitude will be given by

$$\beta_h = \frac{G_T \cdot L_o}{G_{Bh}} \quad .. \quad .. \quad .. \quad (7)$$

and at ground level it will be $\beta_o = \dfrac{G_T \cdot L_o}{G_{Bo}}$ .. (8)

By equating the expressions (7) and (8) we obtain

$$\frac{\beta_h}{\beta_o} = \frac{G_{Bo}}{G_{Bh}} \text{ where } \frac{G_{Bh}}{G_{Bo}} = \frac{\eta_{vh} \cdot \gamma_h}{\eta_{vo} \cdot \gamma_o} = \Delta.$$

$$\text{Therefore, } \beta_h = \frac{\beta_o}{\Delta} \quad .. \quad .. \quad .. \quad (9)$$

$$\text{But since } \frac{(\beta\eta_1)_h}{(\beta\eta_1)_o} \approx \frac{4.77 - \dfrac{1}{\beta_h}}{4.77 - \dfrac{1}{\beta_o}} \quad .. \quad (10)$$

equation (9) can be also written

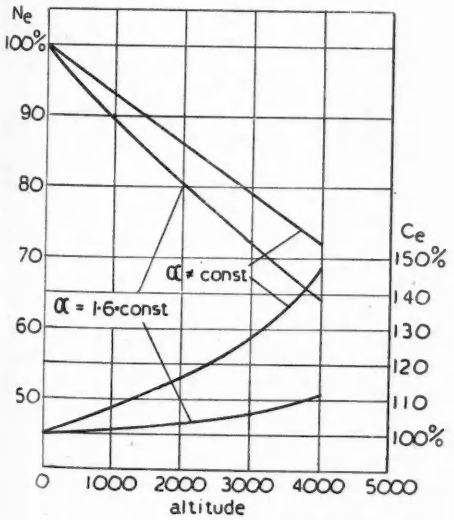

Fig. 6. **Variation in engine output and specific fuel consumption with the altitude for either β = const. or $\beta \neq$ const.**

$$\frac{(\beta\eta_1)_h}{(\beta\eta_1)_o} \approx \frac{4.77 - \dfrac{\Delta}{\beta_o}}{4.77 - \dfrac{1}{\beta_o}} = \frac{4.77 \cdot \beta_o - \Delta}{4.77\,\beta_o - 1} \quad .. \quad (11)$$

Since for n = constant and β = constant, $N_i = k\,\beta\eta_i\,\eta_v\,\eta_h$, and the equations (1) and (11) can be used to express the functionality of the variation in indicated output with the altitude by means of the relation

$$\frac{N_{ih}}{N_{io}} = \frac{4.77\,\beta_o - \Delta}{4.77\,\beta_o - 1}\Delta \quad .. \quad .. \quad (12)$$

If it is assumed that $N_{rh} = N_{ro}$ = const., the effective output at altitude can be expressed by

$$N_{eh} = N_{ih} - N_{rh} = N_{io}\frac{4.77\,\beta_o - \Delta}{4.77\,\beta_o - 1}\Delta - N_{ro} \quad (13)$$

$$\text{or } N_{eh} = N_{eo}\frac{\Delta}{\eta_{mo}}\frac{4.77\,\beta_o - \Delta}{4.77\,\beta_o - 1} - N_{eo}\left(\frac{1}{\eta_{mo}} - 1\right) \quad (14)$$

and finally

$$N_{eh} = N_{eo}\left[\frac{\Delta}{\eta_{mo}}\frac{4.77 \cdot \beta_o - \Delta}{4.77\,\beta_o - 1} - \left(\frac{1}{\eta_{mo}} - 1\right)\right] \quad (15)$$

$$\text{Making } B = \frac{\Delta}{\eta_{mo}}\frac{4.77\,\beta_o - \Delta}{4.77\,\beta_o - 1} - \left(\frac{1}{\eta_{mo}} - 1\right) \quad (16)$$

we have $N_{eh} = B\,N_{eo}$ .. .. .. (17)

For $\eta_{mo} = 0.85$ it is

$$B = 1.18\Delta\frac{4.77\,\beta_o - \Delta}{4.77\,\beta_o - 1} - 0.18 \quad .. \quad (18)$$

As $\Delta < 1$, a comparison of (18) and (4) will show that $B > A$. Therefore, if β is variable, the engine output will fall with the altitude at a noticeably slower rate than if β were kept constant.

The respective variations of engine power and specific fuel consumption with the altitude at constant engine speed for $\beta \neq$ constant and β = constant are given in Fig. 6, the basic value of β being $\beta_o \approx 0.63$ ($\alpha = 1.6$). It was mentioned before that with $\beta \neq$ *constant* the ceiling height is given by the max. value of $\beta = \beta_{max}$ that can be obtained. At altitudes exceeding this ceiling, β_{max} will remain constant and the computation of engine output and fuel consumption must then be based upon the equations established for β = constant. The maximum value for β that can be obtained with present day engines will hardly exceed $\beta_{max} = 0.8$.

Computations as well as tests have shown that with an engine laid out for G_T = constant, at a certain altitude the power output at unchanged speed will exceed power requirements if an air screw with fixed blades is used. This excess power will lead to an increase in engine speed. In the case of a variable pitch propeller, the pitch must be increased until a height is reached where n_{max} and β_{max} cannot be any more obtained. Any further climbing of the plane will lead to a faster decrease in engine power than is required by the air screw. Consequently, the speed of the air screw will decrease, and at a certain height it will *turn* at its nominal speed; beyond this, the speed of the air screw will further decrease. This process is illustrated in Fig. 7, where curve (1) represents the variation in effective power with the altitude with β_o and n_o = constant. Curve (2) shows the power requirements of the air screw with fixed blades at constant speed n_o as function of the altitude. Curve (6) gives the variation in engine speed, and curve (4) shows the variation in power output if

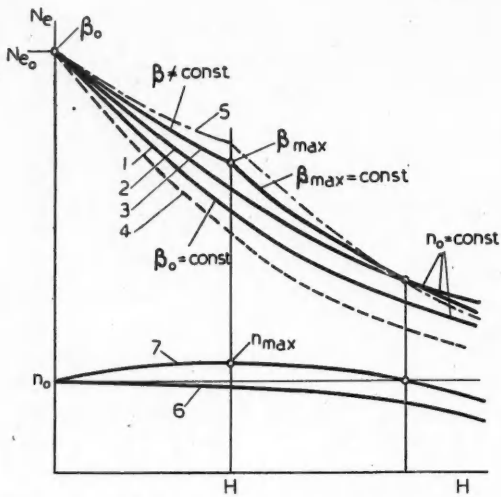

Fig. 7. Variation in engine output and propeller speed for either $\beta \neq$ const. or β = const.

β_o remains constant. Curve (3) shows the variation in engine output up to a certain altitude H corresponding to β_{max}, G_T being kept at constant and β being varied. For higher altitudes β_{max} remains constant and G_T varies. The variation in engine speed is given by curve (7). Finally curve (5) shows the variation in power output with the height if β is variable.

The chart shown in Fig. 8 was derived from an actual altitude test of a Packard aviation Diesel engine and of two Otto engines. It shows that the decrease in engine power with the height is smaller for a Diesel than for an Otto engine. In the case of a four-stroke cycle aviation Diesel engine for altitude operation, the charging pressure p_k is kept constant up to the specified altitude. At greater heights the engine may be operated within certain limits with a variable β value.

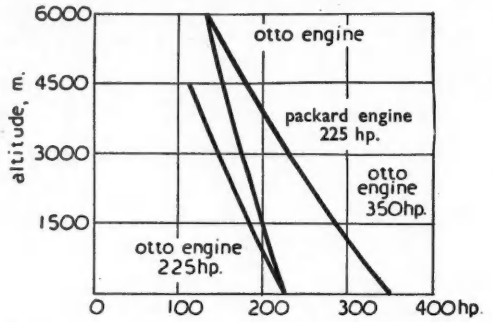

Fig. 8. Altitude characteristics of Packard Diesel engine and two Otto engines of 225 and 350 h.p. respectively.

EXHAUSTING AND SCAVENGING OF THE TWO-STROKE DIESEL ENGINE.

In general the pressure decrease during the exhaust period prior to the commencement of scavenging may lie either above or below the critical pressure range, and the changes in the condition of the gas may be assumed to proceed polytropically.

If p_b and v_b are the pressure and the specific volume respectively of the products of combustion at the end of the expansion period coincident with the opening of the exhaust organ, then

$$\frac{p_1}{v_1} = \frac{p_b}{v_b}\left(\frac{p_1}{p_b}\right)^{\frac{m+1}{m}} \quad .. \quad .. \quad (19)$$

$$\text{Also } d\,G = \mu_B f \psi \sqrt{\frac{p_b}{v_b}} \left(\frac{p_1}{p_b}\right)^{\frac{m+1}{m}} dt \quad .. \quad (20)$$

$$\text{where } \psi = \sqrt{2g \frac{k}{k-1}\left[\left(\frac{p}{p_1}\right)^{\frac{2}{k}} - \left(\frac{p}{p_1}\right)^{\frac{k+1}{k}}\right]} \quad (20a)$$

The decrease in the weight of gas contained in the cylinder after a time Δt is given by $\Delta G = \frac{V_1}{v_1} - \frac{V_1}{v_1}$ where V_1 and V_1 are the initial and final cylinder volumes and v_1 and v_1 are the specific volumes of the gas respectively.

The following differential equation therefore, obtains :

$$d\,G = -\frac{1}{v_b} d\left[V_1\left(\frac{p_1}{p_b}\right)^{\frac{1}{m}}\right] \quad .. \quad (21)$$

By equating the expressions (20) and (21) it is found

$$\mu_B . f . \psi \sqrt{\frac{p_b}{v_b}} \left(\frac{p_1}{p_b}\right)^{\frac{m+1}{2m}} dt = -\frac{1}{v_b} d\left[V_1\left(\frac{p_1}{p_b}\right)^{\frac{1}{m}}\right] \quad (22)$$

As

$$d\left[V_1\left(\frac{p_1}{p_b}\right)^{\frac{1}{m}}\right] = \left(\frac{p_1}{p_b}\right)^{\frac{1}{m}} d\,V_1 + \frac{1}{m} V_1 \left(\frac{p_1}{p_b}\right)^{\frac{1}{m}-1} d\left(\frac{p_1}{p_b}\right) \quad (23)$$

$$\text{Also } \frac{f\,d\,t}{V_1} = -\frac{1}{m\,\mu_B\,\psi\sqrt{p_b\,v_b}}\left(\frac{p_1}{p_b}\right)^{\frac{1}{2m}-\frac{3}{2}} . d\left(\frac{p_1}{p_b}\right) - \frac{1}{\mu_B\,\psi\sqrt{p_b\,.\,v_b}} \cdot \frac{1}{\left(\frac{p_1}{p_b}\right)^{\frac{1}{2}-\frac{1}{2m}}} \cdot \frac{d\,V_1}{V_1} \quad .. \quad (24)$$

The variable cylinder volume V_1 may be taken as approximately constant and equal to the arithmetic mean value of V_b and V_m at the commencement and ending of the first phase respectuvely, that is to say

$$V = \frac{V_b + V_m}{2}$$

The length of time required for the process of exhausting up to commencement of scavenging is therefore given by

$$A_0 = \int_0^{t_0} f\,dt = -\frac{V}{m\,\mu_B\sqrt{p_b\,v_b}} \int_1^{\frac{p_m}{p_b}} \frac{\left(\frac{p_1}{p_b}\right)^{\frac{1}{2m}-\frac{3}{2}}}{\psi} d\left(\frac{p_1}{p_b}\right) - \frac{1}{\mu_B\sqrt{p_b\,v_b}} \int_{V_b}^{V_m} \frac{dV_1}{\psi\left(\frac{p_1}{p_b}\right)^{\frac{1}{2}-\frac{1}{2m}}} \quad .. \quad (25)$$

Generally, if evacuation of the gases from the cylinder takes place both above and below the critical pressure, the integral of the first member of equation (25) can be replaced by two integrals. The first of these refers to the range above the critical pressure from $\frac{p_b}{p_b} = 1$ to $\frac{p_{kp}}{p_b}$ where $\psi = \psi_{max} =$ constant ; while the second integral refers to the range below the critical pressure delimited by $\frac{p_{kp}}{p_{kp}} = 1$ and $\frac{p_m}{p_{kp}}$ where ψ is a variable. As the second integral is small compared to the first one, A. S. Orlin has suggested that for the first

integral $\psi = \psi_{max}$ may be assumed as constant.

In the general case we therefore obtain

$$A_0 = A_0' + A_0'' + A_0''' = -$$

$$-\frac{V}{m\mu_B \psi_{max}\sqrt{p_b v_b}} \int_1^{\frac{p_{kp}}{p_b}} \left(\frac{p_l}{p_p}\right)^{\frac{1}{2m}-\frac{3}{2}} d\left(\frac{p_l}{p_b}\right) -$$

$$-\frac{V}{m\mu_B \sqrt{p_{kp} v_{kp}}} \int_1^{\frac{p_m}{p_{kp}}} \frac{1}{\psi}\left(\frac{p_l}{p_{kp}}\right)^{\frac{1}{2m}-\frac{3}{2}} d\left(\frac{p_l}{p_{kp}}\right) -$$

$$-\frac{1}{\psi_{max}\mu_B\sqrt{p_b v_b}} \int_{V_b}^{V_m} \frac{dV_l}{\left(\frac{p_l}{p_b}\right)^{\frac{1}{2}-\frac{1}{2m}}} \quad .. \quad (26)$$

If p_p is the pressure in the exhaust pipe, then

$$p_{kp} = p_p \left(\frac{k+1}{2}\right)^{\frac{k}{k-1}}$$

Upon interpretation the first member of the right hand side of equation (26) can be written as

$$A_0' = -\frac{V}{m\mu_B\psi_{max}\sqrt{p_b v_b}} \int_1^{\frac{p_p}{p_b}\left(\frac{k+1}{2}\right)^{\frac{k}{k-1}}} \left(\frac{p_l}{p_b}\right)^{\frac{1}{2m}-\frac{3}{2}} d\left(\frac{p_l}{p_b}\right) =$$

$$= \frac{2}{m-1} \cdot \frac{V}{\mu_B\sqrt{p_b v_b}\left(\frac{2}{k+1}\right)^{\frac{1}{k-1}}\sqrt{\frac{2gk}{k+1}}} \left[\left(\frac{k+1}{2}\right)^{\frac{k}{k-1}\cdot\frac{1-m}{2m}} \times \left(\frac{p_b}{p_p}\right)^{\frac{m-1}{2m}} - 1\right] \quad (27)$$

Assuming $m = k = 1.3$ and replacing $p_b v_b$ by RT_b, we obtain

$$A_0' = \frac{0.59\ V}{\mu_B\sqrt{T_B}}\left[0.932\left(\frac{p_b}{p_p}\right)^{0.115} - 1\right] \quad .. \quad (28)$$

The second integral of equation (26) requires special treatment. We can write

$$\frac{p_l}{p_{kp}} = \frac{p_l}{p_p}\cdot\frac{p_p}{p_{kp}} = \left(\frac{p_p}{p_l}\right)^{-1}\frac{p_p}{p_{kp}} \quad .. \quad (29)$$

and therefore

$$d\left(\frac{p_l}{p_{kp}}\right) = -\frac{p_p}{p_{kp}}\left(\frac{p_p}{p_l}\right)^{-2} d\left(\frac{p_p}{p_l}\right) \quad .. \quad (30)$$

On this basis the second integral of equation (26) can be written

$$A_0'' = -\frac{V}{m\mu_B\sqrt{p_{kp}v_{kp}}} \int_{\frac{p_p}{p_{kp}}}^{\frac{p_p}{p_m}} \frac{1}{\psi}\left[\left(\frac{p_p}{p_l}\right)^{-1}\frac{p_p}{p_{kp}}\right]^{\frac{1}{2m}-\frac{3}{2}} \times \left(-\frac{p_p}{p_{kp}}\right)\left(\frac{p_p}{p_l}\right)^{-2} d\left(\frac{p_p}{p_l}\right) =$$

$$= \frac{V}{m\mu_B\sqrt{p_{kp}v_{kp}}}\left(\frac{p_p}{p_{kp}}\right)^{\frac{1}{2m}-\frac{1}{2}} \int_{\frac{p_p}{p_{kp}}}^{\frac{p_p}{p_m}} \frac{1}{\psi}\left(\frac{p_p}{p_l}\right)^{-\frac{1}{2m}-\frac{1}{2}} d\left(\frac{p_p}{p_l}\right) \quad (31)$$

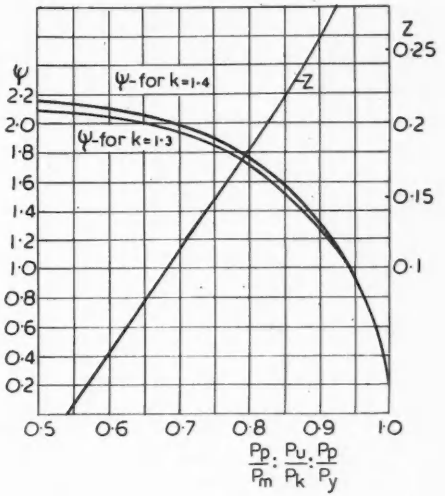

Fig. 9. **Values for ψ and Z** *versus* $\frac{P_p}{p_m}$, $\frac{P_z}{p_k}$, and $\frac{P_p}{p_z}$.

so that

$$A_0'' = \frac{V}{m\mu_B\sqrt{RT_{kp}}}\left(\frac{k+1}{2}\right)^{\frac{k}{k-1}\cdot\frac{m-1}{2m}} Z, \quad .. \quad (32)$$

where

$$Z = \int_{\frac{p_p}{p_{kp}}}^{\frac{p_p}{p_m}} \frac{1}{\psi}\left(\frac{p_p}{p_l}\right)^{\frac{1-m}{2m}} d\left(\frac{p_p}{p_l}\right) = f\left(\frac{p_p}{p_m}\right). \quad .. \quad (33)$$

Values of the variable ψ for values of $k = 1.3$ and $k = 1.4$ are plotted in Fig. 9. This chart also gives Z as function of $\frac{p_p}{p_m}$.

Taking $m = k = 1.3$, $R = 29.3$ and expressing T_{kr} by the temperature T_b by means of the polytropic relationship, we obtain

$$T_{kp} = T_b\left(\frac{p_{kp}}{p_b}\right)^{\frac{m-1}{m}} = T_b\left[\frac{p_p}{p_b}\left(\frac{k+1}{2}\right)^{\frac{k}{k-1}}\right]^{\frac{m-1}{m}} =$$

$$= 1{,}15\,T_b\left(\frac{p_p}{p_b}\right)^{0{,}231} \quad (34)$$

Equation (32) can therefore be given as

$$A_0'' = \frac{0.143\ V}{\mu_B\sqrt{T_b}}\left(\frac{p_b}{p_p}\right)^{0.115} Z \quad .. \quad (35)$$

According to Orlin it can be written

$$\int_{V_b}^{V_m} \frac{dV_l}{\left(\frac{P_l}{p_b}\right)^{\frac{1}{2}-\frac{1}{2m}}} \simeq 1.05\ V \log_e \frac{V_m}{V_b} \quad .. \quad (36)$$

and the third member of equation (26) can therefore be written

$$A_0''' = -\frac{1.05\ V}{\mu_B\psi_{max}\sqrt{RT_b}}\log_e\frac{V_m}{V_b} = -\frac{0.093\ V}{\mu_B\sqrt{T_b}}\log_e\frac{V_m}{V_b} \quad .. \quad (37)$$

With the use of equations (28), (35) and (37) the expression for A_o can now be established as follows:

$$A_o = \frac{0.143}{\mu_B \sqrt{T_b}} V \left[\left(\frac{p_b}{p_p}\right)^{0.115} (3.86 + Z) - \right.$$
$$\left. - 4.14 - 0.65 \log_e \frac{V_m}{V_b} \right] \quad .. \quad (38)$$

If $p_m \geq p_{kp}$, it becomes $A_o'' = O$, and the expression (38) takes the form

$$A_o = A_o' + A_o'' = \frac{0.143}{\mu \sqrt{T_b}} V \left[4.14 \left(\frac{p_b}{p_m}\right)^{0.115} - \right.$$
$$\left. - 4.14 - 0.65 \log_e \frac{V_m}{V_b} \right] \quad .. \quad (39)$$

where

$$A_o' = \frac{V}{m \mu_B \psi_{max} \sqrt{p_b v_b}} \int_I^{p_m/p_b} \left(\frac{p_1}{p_b}\right)^{\frac{1}{2m} - \frac{3}{2}} . d \left(\frac{P_1}{p_b}\right)$$
$$= \frac{0.59 V}{\mu_B \sqrt{T_b}} \left[\left(\frac{p_b}{p_m}\right)^{0.115} - 1 \right] \quad .. \quad (40)$$

For two-stroke engines running at high speed the pressure p_m in the cylinder amounts to 2–3 atm. when scavenging begins. For this case the time A_o of the first phase can be computed with the use of equation (40). In order to be able to compute A_o, the factors p_b, T_b, p_p, p_m, μ, V_b and V_m must be known. The pressure p_b and the temperature T_b at the end of the expansion are known from thermal computation, or they may be given, the temperature T_b, for instance, ranging from 1200–1400 deg. K. The coefficient μ_B can be assumed to lie between 0.65–0.8, and $p_m = p_k + (0.2 \div 0.5)$ kg. per sq. cm. where p_k is the receiver pressure of the scavenger air. The pressure p_p is found as $p_H + (0.2 \div 0.3)$ kg. per sq. cm. if exhaust to atmosphere takes place. If an exhaust turbine is provided, the pressure p_p must be found from the Rateau equation. The factor V_b referring to the termination of expansion is known, and so is also V_m. Errors made in the fixing of values for T_b and V_m will affect but little the results of the computation.

It may be assumed that during the entire process of scavenging the pressure p_k in the scavenge air receiver remains constant and that the pressure in the cylinder likewise remains constant and has a certain mean value p_z. These assumptions imply that the scavenge air is passed from the receiver into the cylinder with a constant pressure differential. Computation of the time requirements is, therefore, an easy matter. However, this assumption of constant pressures p_k and p_z does not correspond to actual conditions where pressure fluctuations occur owing to irregularities in the flow of the gases in the cylinder and from the cylinder into the exhaust pipe.

THE SCAVENGING PROCESS.

We proceed from the basic equation

$$f\,dt = \frac{d\,G}{\mu_{II}\ \psi_{II} \sqrt{\frac{p_k}{V_k}}} \quad .. \quad .. \quad .. \quad (41)$$

where p_k and v_k are the pressure and the specific volume respectively which prevail in the scavenge air receiver, and μ_{II} is the coefficient of discharge of the scavenging port. The factor ψ_{II} is given by the expression

$$\psi_{II} = \sqrt{2\,g \frac{k}{k-1} \left[\left(\frac{pz}{p_k}\right)^{\frac{2}{k}} - \left(\frac{pz}{pk}\right)^{\frac{k+1}{k}} \right]} = \text{const.} \quad (42)$$

By integrating equation (41) within the range $t_o - t_1$, the time required for scavenging is found as

$$A_1 = \int_{t_o}^{t_1} f\,dt = \int_o^{G_k} \frac{d\,G}{\mu_{II}\ \psi_{II} \sqrt{\frac{p_k}{V_k}}} = \frac{G_k}{\mu_{II}\ \psi_{II} \sqrt{\frac{p_k}{V_k}}} \quad (43)$$

The amount of air admitted through the scavenging port during the process of scavenging is given by

$$G_k = \frac{\eta_v V_h}{v_k} \varphi_k \quad .. \quad .. \quad (44)$$

where V_h is either the working or the total cylinder volume, and η_v is the coefficient of volumetric efficiency based on either the working volume or on the total volume of the cylinder. By introducing the value for G_k, as given by expression (44) into equation (43), it becomes

$$A_1 = \frac{\eta_v V_h \varphi_k}{\mu_{II}\ \psi_{II} \sqrt{p_k v_k}} = 0.185 \frac{\eta_v V_h . \varphi_k}{\mu_{II}\ \psi_{II} \sqrt{T_k}} \quad (45)$$

where T_k is the temperature of the scavenge air. This temperature T_k is either known from test, or it can be obtained from the expression

$$T_k = T_h \left[1 + \frac{\left(\frac{p_k}{p_h}\right)^{\frac{k-1}{k}} - 1}{\eta\ a\ d} \right] \quad .. \quad (46)$$

The product $\eta_v V_h \varphi_k$ is also either known, or it can be determined by computation. The factor ψ_{II} can be obtained from Fig. 9 if the ratio $\frac{p_z}{p_k}$ is known. The pressure p_k of course is always known, and the pressure p_z can be computed from

$$p_z = p_p + 0.35\,(p_k - p_p) \quad .. \quad (47)$$

The time required for exhausting during the scavenging process can be easily computed as the pressure difference $p_z - p_p$ prevailing between the cylinder and the exhaust pipe is assumed to be constant. In this case the time required for evacuation during the scavenging process is given by

$$A_2 = \int_{t_0}^{t_1} f\,.\,dt = \int_o^{G_r} \frac{d\,G}{\mu_B\ \psi_B} \sqrt{\frac{p_z}{Vz}} \quad .. \quad (48)$$

$$\psi_B = \sqrt{2\,g \frac{k}{k-1} \left[\left(\frac{p_p}{p_z}\right)^{\frac{2}{k}} - \left(\frac{p_p}{p_z}\right)^{\frac{k+1}{k}} \right]} = \text{constant} \quad (49)$$

The factor ψ_B can also be read off in the chart (Fig. 9) for a given value of $\frac{p_p}{p_z}$.

If the average pressure p_z in the cylinder is taken as constant during the scavenging process, the specific volume v_z can also be taken as constant; and therefore

$$A_2 = \frac{Gr}{\mu_B\ \psi_B \sqrt{\frac{p_z}{v_z}}} \quad .. \quad .. \quad (50)$$

(*To be continued*).

BRAKING AIRSCREW AND HIGH SPEED FLIGHT.

By Dipl. Ing. A. VON DER MÜHLL, Airscrew Division of the Escher Wyss Co., Zurich. (From *Flugwehr und Technik*, No. 7, July, 1944, pp. 199-202).

(*Continued from the previous issue of* THE ENGINEERS' DIGEST).

THE MAXIMUM HORIZONTAL SPEED.

THE following is based on a lecture by Prof. Dr. F. Ackeret, delivered in 1935 at the Swiss Federal Technical College (E.T.H.).

To estimate the maximum horizontal speed the equation expressing equilibrium in the horizontal direction is to be divided by that for equilibrium in the vertical direction. Hence—

$$V_{h\ max} = \frac{N_e}{G} \cdot \frac{\eta}{\epsilon} \quad .. \quad .. \quad .. \quad (7)$$

According to this simple relationship the maximum horizontal spread is inversely proportional to the power loading $\frac{G}{N_e}$ and the gliding angle ϵ.

$$\left(\epsilon = \frac{W}{A} = \frac{C_w}{C_a}, \text{ Fig. 1.} \right)$$

Assume an aircraft having the following data :

Weight G = 3000 kg.
Airscrew efficiency $\eta = 0.80$
Engine power N = 1500 h.p.

From the polare we obtain the aerodynamic coefficients (Fig. 2).

Optimum gliding angle $\epsilon_{min} = 0.0712$
Lift coefficient $C_a = 0.7$
Drag coefficient $C_w = 0.0498$

The maximum horizontal speed for this aircraft is

$$V_{h\,max} = \frac{1500 \times 75}{3000} \cdot \frac{0.80}{0.0712} = 422 \text{ m./sec.} = 1520 \text{ km./hr.}$$

Such a speed cannot be realized, as not only the horizontal but also the vertical equilibrium condition must be satisfied. Assuming for instance a wing loading G/F = 220 kg./sq. m. for the above aircraft, the density can be calculated which satisfies the equation $G = A = C_a (\rho/2) V^2 . F$. This density is $\rho = 0.00353$ kg. sec.^{2}/m^4, and the corresponding altitude in H = 25.9 km. At such an altitude it is not possible to maintain sea-level engine power. Taking present possibilities into account, a maximum rated altitude of H = 7 km. ($\rho = 0.06$) would necessitate a wing loading of G/F = 3740 kg./sq. m. This high value (the wing area would be less than 1 sq. m.), is just as impossible to attain as is the altitude of 25.9 km. Further, additional limitations, mainly the influence of compressibility, the reduction of Reynolds' number with decreasing density, make it impossible to realize the calculated speed at present. Nevertheless, eq. (7) gives a clear indication as to the factors contributing to a possible speed increase. Of these a minimum gliding angle is the more important as it is simultaneously a condition for maximum range.

INCREASE IN MAXIMUM SPEED.

For a given total aircraft weight and given airfoil section (i.e., the maximum lift available with a chosen landing flap), the wing area can be calculated when the allowable landing speed has been fixed.

$$\text{Thus, } F = \frac{G}{\rho_L/2 \, . \, C_{aL} \, . \, V_L^2}, \quad .. \quad .. \quad (2a)$$

a relationship already stated by eq. (2). Substituting eq. (2a) into eq. (3a) the maximum horizontal speed is obtained :

$$V_h = \sqrt[3]{\frac{N \eta_h}{G} \cdot \frac{\rho_L}{\rho_h} \cdot \frac{C_{aL}}{C_{wh}} \cdot V_L^2} \quad .. \quad (8)$$

This is the maximum speed which can be reached by taking into account the fact that the aircraft is earth-bound, i.e., that an allowable landing speed must not be exceeded. Under these conditions an increase in maximum horizontal speed is obtainable by the following means :

(1) Increased engine power N.
(2) Increased airscrew efficiency η_h.
(3) Reduction of structural weight G.
(4) Increase of altitude to increase the ratio ρ_L/ρ_h.
(5) Increased maximum lift coefficient C_{aL}.
(6) Reduction of drag coefficient at high speed C_{wh}.
(7) Increased landing speed V_L.

Let us now review the possibilities in the light of the recent advances in airscrew design.

(1) Increased power without weight increase can be expected in the future by two-stroke combustion engine and jet power units. A limit is set to power increase by the increase of fuel consumption as soon as the question of range has to be considered.

(2) Propulsive efficiency now exceeds 80 per cent the efficiency of 90 per cent—not impossible when using control rotating variable pitch airscrews—would increase the maximum speed by a mere 4 per cent. Jet propulsion at subsonic speeds does not seem to offer an improvement when relating the propulsive efficiency to fuel consumption.

(3) Structural weight of high speed aircraft is at present determined by problems of vibration (flutter). It is unlikely that current weights could essentially be reduced.

(4) The increase of altitude beyond 6 or 7 km. necessitates the use of pressurized cabins which introduction makes for increase in structural weight. As, however, the compressibility effect is sooner present at high altitude, the increase of altitude is bound to lead to difficulties.

(5) The maximum lift coefficient could only be increased by special means such as boundary layer control. These are not yet practically applicable and are disregarded here.

(6) To reduce the drag of streamline bodies and airfoils the maintenance of the laminar boundary layer is essential. It is hoped that in the near future two developments will mature to practical applicability [6]*. A great reduction in total drag can be achieved by decreasing the wing area. This leads to the next point.

(7) The increase of landing speed. In eq. (8) the landing speed V_L is the only value under the cubic root which is squared. This suggests that an increase of the landing speed is the most effective of all possible improvements. Let us discuss this possibility more fully.

THE MAXIMUM SPEED AS A FUNCTION OF LANDING SPEED.

Using the formula eq. (8) it can be calculated that by increasing the landing speed from the present value of 130 km./hr. to 200 km./hr., the maximum horizontal speed increases by about one third. All the other aircraft data are assumed to remain unchanged. The actual gain in speed will be smaller than suggested by eq. (8) as the aerodynamic fineness of an aircraft decreases with decreasing wing area. With a smaller

wing the parasite drag relative to the wing area increases. Only with aircraft of much larger size than those built at present can the ideal case, i.e., the all wing aircraft, be obtained, which is independent of the magnitude of the wing loading insofar that there is no parasite drag. With present day fast aircraft where the wing drag is about half the total drag, the reduction of the wing surface to decrease wing drag is still a very advantageous method. The relevant problems are discussed by Belart [5] and need not be repeated here.

Owing to the detrimental effect of compressibility at high speeds, the speed gain due to increase in wing loading is once more reduced. (This reduction applies to values calculated by eq. (8) and to the results of ref. [5].)

As it is difficult to show the effect of compressibility in a closed form, an example has been chosen which will illustrate the gain in speed due to increase of wing loading while taking into account all reduction factors (including *inter alia* the compressibility effect on the airscrew and the interaction between wing and fuselage).

The example is based on the following assumptions :

The wing area of a given type of high-speed aircraft should be changed so that the landing speed varies from 50 to 250 km./hr., when

(a) the parasite drag (fuselage, cooler, etc.), is taken as constant ;
(b) the total weight G = 3000 kg. is independent of the wing area ;
(c) the aspect ratio A = const. = 8.
(d) the lift coefficient at landing C_{aL} = const. = 1.75.

For each wing an exact polare has been drawn and for the available airscrew curves the maximum speed in three altitudes has been calculated. The calculations were made for various wing loadings, G/N = 4, 3.5, 3, 2.5, 2, 1.5 and 1.25 kg./h.p. (according to the engine power of 750, 860, 1000, 1200, 1500, 2000 and 2400 h.p.). The results are given in Figs. 4, 5 and 6. It can be seen that for each wing loading the maximum speed occurs at landing speeds between 200 and 250 km. It is, therefore, of advantage to employ such high landing speeds as they are possible by using braking airscrews.

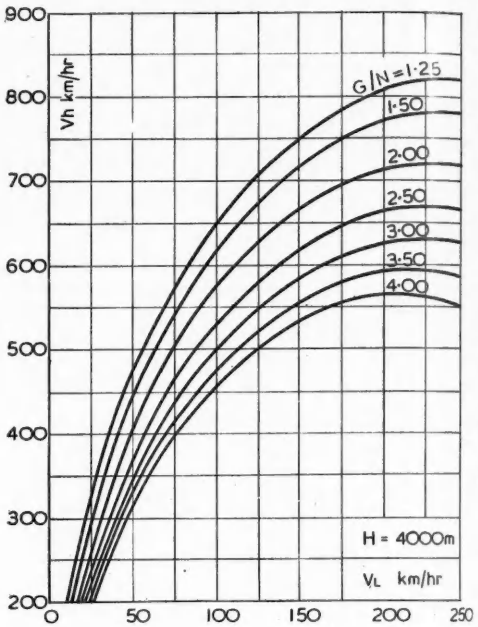

Fig. 5

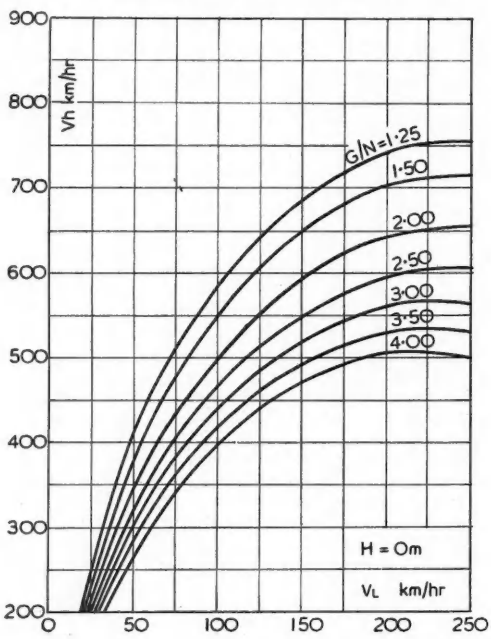

Fig. 4

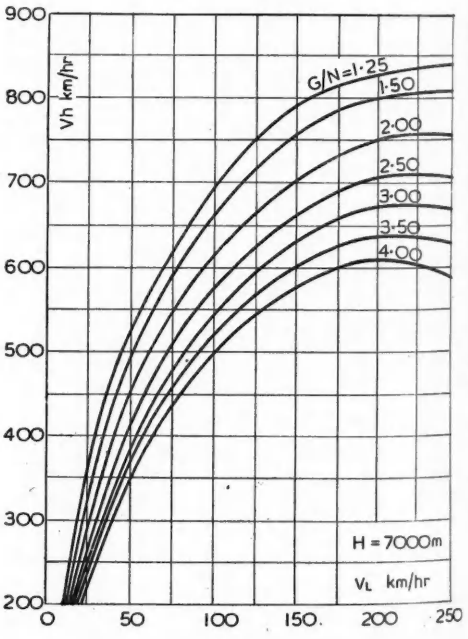

Fig. 6

Figs. 4, 5 and 6. Maximum speed as a function of landing speed for various wing loadings.

To increase the landing speed from its standard value of 130 km./hr. to about 200 km./hr., means—without changing the engine power—an increase in maximum speed by 11 per cent at 7000 m. altitude, by 12.5 per cent at 4000 m., and by 14 per cent at sea level. With the present value of the landing speed such a speed increase would require 50 per cent greater engine power, whereby fuel consumption would increase accordingly, and consequently the range would decrease. Therefore, the advantage of high landing speed is proved beyond doubt. That such high landing speeds are feasible has already been shown in reference [2].

An advantage of the outlined development lies in the fact that the adoption of higher landing speeds with existing aircraft does not require any other change than a reduction of the wing area and the installation of the braking airscrew (see Fig. 7). The important advantages of high wing loadings is that they permit high speed to be coupled with great range, and thus contribute to economy which offers new possibilities for future air transport.

*Numerals in brackets [ ] indicate literature references at the end of the first instalment of this article.

Fig. 7. **Model of a high-speed aircraft according to the author's proposals (top) compared with that of a present-day aircraft (bottom).**

THE RECOVERY OF HARD METAL FROM GRINDING DUST AND GRINDING SLUDGE.

By Dr.-Ing. E. DINGLINGER. (From *Werkstattstechnik Der Betrieb*, Vols. 37/22, No. 5, May, 1943, pp. 181-183).

IN new processes and operations, workshops are now turning over to the use of hard metal tools which permit six to ten times the previous output to be obtained. The original field of application of hard metals is expanding continuously and the production capacity of our armament industry goes on mounting rapidly. The increasing consumption of hard metal makes it incumbent to recover, so far as possible, the valuable sintered metal which contains 80 per cent to 90 per cent tungsten. For this reason it is necessary to make the collecting of hard metal scrap a particular aim.

Hard metal scrap occurs, as chippings in the manufacture of the tools; when cracked tips are detached; when all remnants or odd pieces of used tools are broken up.

The following recommendations for the collection and utilisation of this hard metal scrap are given:

(a) Collection should be made continuously to a central depot or store
(b) Hard metal salvaged to be graded according to quality, viz.: H1, H2, G1, G2 and G3 qualities collected in one container, and S1, S2, S3, F1 and F2 qualities in a second container and so on.
(c) The containers to be sealed to prevent errors.
(d) Small pieces may be used for smaller tools where possible.
(e) Particular attention should be drawn to collecting, by means of posters and leaflets.
(f) Scrap from hard metal tools should be returned to the manufacturers.

As approximately 8 per cent to 10 per cent of hard metal occurs as scrap in the form of chippings or scrap from machining, it can be reckoned that this quantity will occur with each fresh delivery.

The remaining portion of the hard metal is not worn away in the actual cutting work (this only blunts the edges), but in sharpening. A considerable quantity of hard metal finds its way into grinding sludge each month.

Investigations show that the separation of silicon carbide from grinding sludge is possible. Difficulty was experienced in defraying the collecting and freight charges, as the value of the yield (12 marks per kilo of hard metal scrap) did not cover these costs. Recent utilization of silicon carbide grinding sludge has now removed that difficulty. For instance, the abrasive industry, the ceramic industry and others use the proceeds from these grindings which fully compensate for the charges.

The point when collecting silicon carbide from wet grinding is to collect the greatest quantity at one time. It is important to know where the hard metal dust settles. Otherwise there is the danger that this important constituent may not be trapped in the recovery process. Hard metal dust settles, on account of their fine grain, not first but last (in spite of their high specific gravity), and in the remotest places of the collecting equipment.

The recovery of hard metal is possible in both dry and wet grinding.

Conditions in high-speed tool grinding are similar, but simpler, for the iron grindings are deposited before the hard metal grindings, so that the danger of loss is not present to the extent it is with hard metal.

DUST SUCTION IN DRY GRINDING.

The grinding points are attached to a common suction plant (Fig. 1). The grindings, in this example, are separated by a cyclone and two filters. As the weight of the tungsten amounts to many times that of silicon carbide powder, it was originally thought that the harder metal would be found in the dust chamber of the cyclone, and the iron and steel dust in the two filter boxes. Examination, however, has shown that coarse-ground particles preponderate in the cyclone. There is only 0.11 per cent tungsten in the cyclone, whilst in the two filters 1.3 per cent to 1.6 per cent and 3.5 per cent to 4.5 per cent is deposited.

This led to the construction of another suction installation (Fig. 2), in order to ensure the recovery of an even greater percentage of tungsten. Here, the grindings also go through a cyclone first. The cyclone

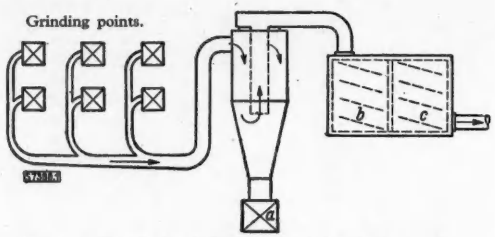

Fig. 1. Lay-out of grinding-dust suction equipment.
Grindings are separated in the cyclone at " a " and in the two filters, " b " and " c " at the back. By far the greatest amount of tungsten is found at " c " and " b."

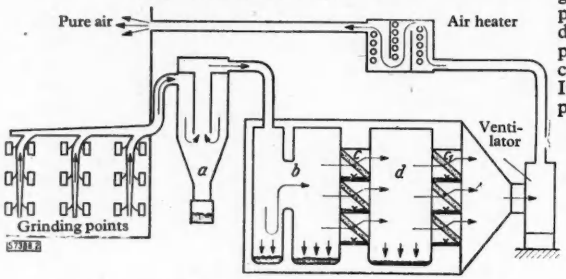

Fig. 2. Construction of an efficient dust extracting apparatus for dry grinding.
(a) Cyclone; (b) ante-chamber for separating, sub-divided by a baffle plate; (cc_1) inclined oil filters (one above the other); (d) second (large) separating chamber; (x) precipitation of grindings containing tungsten.

was found necessary because frequently, through carelessness, larger bodies such as scraps of paper, cleaning rag and cardboard, got into the extractor; these have to be eliminated before they reach the filters to prevent them becoming choked. The dust arrives in an ante-chamber where there is a baffle plate, and from this chamber the dust is sucked through inclined oil filters. It then reaches a further separating chamber and by way of oil filters it enters the ventilator.

In this installation the air sucked in was well cleansed of dust particles. Examination revealed further that in the dust collecting chamber of the cyclone about 0.11 per cent of separated tungsten could again be found. The grindings in the first double chamber contained 1.2 per cent, whilst 9.1 per cent could be determined under the oil filters. Finally, the oil sludge as well, which was deposited in purifying the filters, was examined, and it contained 10.7 per cent tungsten.

Most grindings, viz.: about 90 per cent to 95 per cent of the total quantity obtained are deposited about equally, in this installation, in the ante-chamber in front of the baffle plate, and under the first series of oil filters. In the rear portion of the ante-chamber and in the large chamber between the second series of oil filters only a small proportion of dust is precipitated, just as in the second series of filters there are only a very few dust particles. In case there is not a sufficient market for the utilization of silicon carbide, or if freight conditions preclude all dust being sent to dressing factories, there is only the collection and forwarding of the dust under the first series of filters to deal with. Here, about 70 per cent to 80 per cent of the used hard metal is recovered.

Table 1 gives a comparison of the tungsten content at single dust collecting centres with the findings of three firms in so far as the varying lay-out of the plants permits.

TABLE 1. TUNGSTEN CONTENT OF GRINDINGS IN DRY GRINDING.

Firm	Tungsten content of grindings (weight per cent).			
	In the cyclone	1st chamber	Space under the oil filters (A) or in 2nd chamber (B, C, D)	In the oil of the oil filters
A	0.11	1.2	9.1	10.7
B	—	1.6	3.5	—
C	0.1	1.3	4.5	—
D	—	1.5	1.5	—

SLUDGE DRAINAGE IN WET GRINDING.

For perfect wet grinding it is good if large quantities of water run on to the hard metal job. This requirement is not yet entirely accomplished by the new hard metal grinding machines. Therefore it is expedient for a large tank of pre-heated water to be erected over the grinding machine, this water is fed at a slight incline (if possible without pressure) to the grinding points. It does not circulate because the grindings cannot be perfectly eliminated from it and it is carried off in a common outlet to a preliminary sludge trap (Fig. 3). In the case under examination a second channel is provided outside the workshop as a final sludge trap.

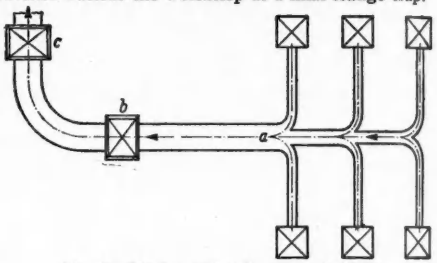

Fig. 3. Sludge outlet in wet grinding.
The sludge settles in the collecting channel at " a " and the sumps " b " and " c_2 " where the flowing speed decreases; tungsten preponderates at " c " and " b."

The sludge at this installation was examined at three points, viz.: at the coalescing of the machine waste water and at the two sludge separators (Fig. 3, a, b, c). The investigation showed at " a " a tungsten content of only 0.34 per cent. In the sludge of the preliminary separator 1.9 per cent was determined, whilst at channel " c " a content of 3.55 per cent was present. It was confirmed that the deposits at the spots remotest from the grinding point contained the most tungsten, whilst the particles of iron grindings were deposited nearer. Table 2 gives a clear synopsis of this.

TABLE 2. ENRICHING OF THE SLUDGE WITH TUNGSTEN AND IRON IN AN INSTALLATION SIMILAR TO FIG. 3.

Metal content per cent	Deposits		
	1	2	3
Tungsten ..	1.45	4.45	6.2
Iron	15.1	6.0	5.1

The result of this investigation shows on the other hand that in collecting hydrosulphuric acid steel grindings the danger of loss is less than in dry grinding. In this type one should see that the first settling tanks are as long as possible, and have a low speed of flow. Sludge research by other firms have ended in similar results (Table 3).

TABLE 3. TUNGSTEN CONTENT (PER CENT) OF THE SLUDGE OF THREE DIFFERENT INSTALLATIONS.

Installation	Deposits		
	1	2	3
A	1.45	4.45	6.2
B	0.67	1.28	6.25
C	1.9	3.55	—

CONSTRUCTION HINTS.

Single Grinding Points.—In grinding plants with only one grinding machine there is a fear that collection would not pay and their hard metal (or high speed steel) grindings would become a loss. To prove the contrary, a simple sludge catch basin with a partition wall was installed (Fig. 4).

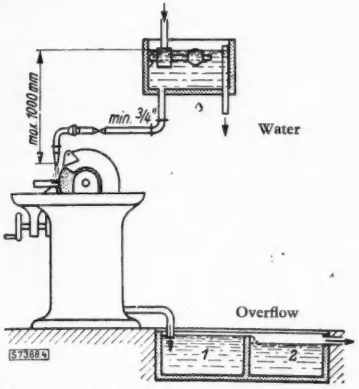

Fig. 4. **Conveying the water for a single grinding point machine.**

It was found that in the first sump 1.45 per cent tungsten was present, and in the second 4.5 per cent. Afterwards a third sump was built and the determination of tungsten found to be as high as 6.2 per cent. In a still more distant spot, no further tungsten was found; the majority of the grindings had settled in the second and third sumps.

The sump, or catch basin, can consist of a simple vessel and the flowing speed must be as low as possible with the water passage as long as possible.

One Common Outlet for Grinding Sludge.—As bigger firms are centralising their tool grinding the result is the erection of more hard metal grinding machines in their works, and it is found best to link them all up to a common sump. When the waste water flows into a collecting channel (Fig. 5) it is easy by providing a flood gate to control the speed of its passage. At the end of this conduit the water is led off through an overflow into a sump or catch basin, and thence into a settling tank. If the results in Table 3 are not uniform, the reason is that the construction of the sumps does not quite correspond with conditions.

Naturally there are exceptions. For instance, grinding sludge from machines which work with a diamond grinding wheel yields a tungsten content of 55.5 per cent, and a cobalt content of 3.2 per cent. In another case, the sludge from a profile grinding machine showed 39.12 per cent tungsten. These special machines should not be attached to the central sludge separation, but arranged apart to transmit the sludge or the dry grindings separately.

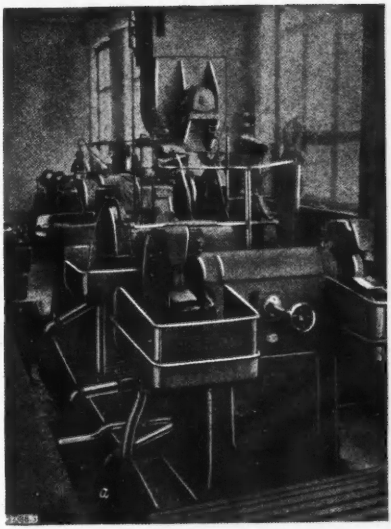

Fig. 5. **Grinding shop with a common water conduit.** (a) Outlet channel.

CORUNDUM POWDER SALVAGE.

In setting up new grinding shops these points should be considered: utilisation of the separated grindings is quicker and more economically feasible if silicon carbide dust and corundum dust are delivered separately. Corundum dust only occurs in shaft grinding machines, and there is no hard metal content in it. The grinding waste water need not, therefore, go through the sumps, and in dry grinding there is no need for a filter installation.

SUMMARY.

The foregoing investigations and experience have shown that by observing a few points without special outlay the recovery of tungsten from grindings can be substantially easier and more economically planned. This can be done in the oldest of existing tool shops. In every factory some little corner could be spared for storage, and it would only need a roof to keep out the rain. If the sludge could be dried artificially transportation would be easier.

Translation by courtesy of Diamond Research Department, 32/34 Holborn Viaduct, London, E.C.1.

THE ADSORPTION OF GASES BY THE STEEL WALLS OF VACUUM DISCHARGE APPARATUS AND ITS BEARING ON THE LIFE OF PUMPLESS MUTATORS

By Dr. W. Deck. (From *Brown Boveri Review*, Vol. 29, No. 8, August, 1942, pp. 202-204).

If a pumpless mutator is heated out at various temperatures and the rate of gas delivery per minute measured, curves similar to those in Fig. 1 are obtained. The quantity of gas given off rises rapidly after each temperature increase, but sinks to low values a few hours later. Even when the tank has been heated for a period of many hours at 500 deg. C., however, the quantity of gas pumped out can still be measured. The same also applies when a well-formed and degassed mutator is subjected to overloads or short circuits in service. The life of a pumpless mutator would therefore be very limited if the steel walls had not a new property, i.e., that of being able to adsorb large quantities of extraneous gases. In contradistinction to X-ray tubes where gas is adsorbed by the electrodes in course of time, the extraneous gases in a mutator are adsorbed less by the electrodes than by the tank walls.

Experiments were carried out with a pumpless test mutator into which known quantities of different gases were introduced (Fig. 2), and the progress of the pressure was followed. The following gases were used for the tests: oxygen, nitrogen, water vapour, hydrogen, carbon monoxide, carbon dioxide, and argon. The three first named gases can find ingress into the mutator through leaky points, the next three are given off by the hot tank walls and electrodes, while argon is employed for filling glow discharge tubes.

Selected test results are illustrated in Figs. 3–6,

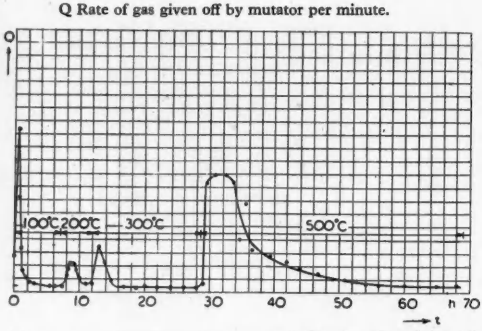

Fig. 1. **Gas given off by a pumpless mutator at various heating temperatures.**

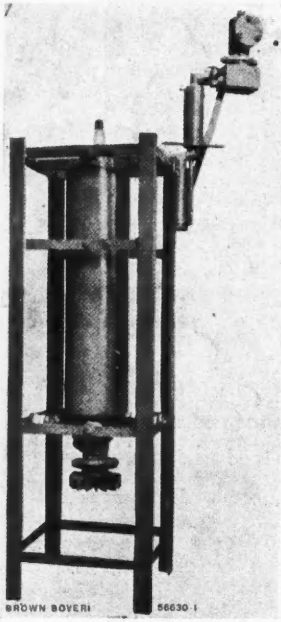

Fig. 2. **Pumpless test mutator**

which show the variation of the pressure of the gases introduced into the test mutator at time O_2 in relation to time. The bold-lined portions of the curves represent the intervals of time during which the mutator was switched in.

N_2, CO, CO_2 and H_2 are not adsorbed by the tank walls until the arc is ignited, and their pressure remains unchanged even after a period of many hours. When the mutator is switched in the gases are adsorbed, the rate of adsorption depending on the nature of the gas. Argon is not affected by the arc (Fig. 3).

O_2 and H_2O are rapidly adsorbed by the tank walls even before the arc is struck. Through the arc the adsorption of O_2 is considerably accelerated, while water vapour is, to a certain extent, again given off.

The tank walls are not able to adsorb any desired quantity of gases. Fig. 5 shows that the pressure of oxygen sinks the slower the more intensively the walls are charged with gas during the previous tests. The Roman figures indicate the order of the tests. In tests I. to III. the adsorption took place without the arc

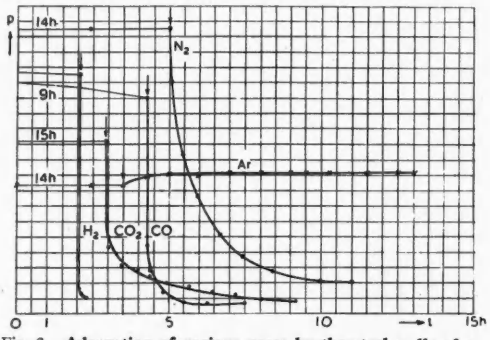

Fig. 3. **Adsorption of various gases by the steel walls of a pumpless mutator.**

↓ = moment of switching in mutator.

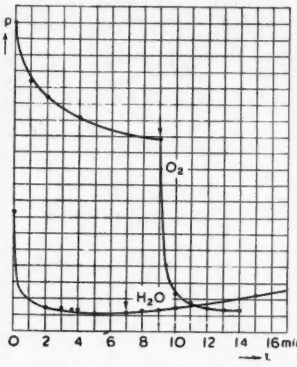

Fig. 4. **Adsorption of oxygen O_2 & water vapour H_2O by the steel walls of a pumpless mutator.**

↓ = moment of switching in mutator.

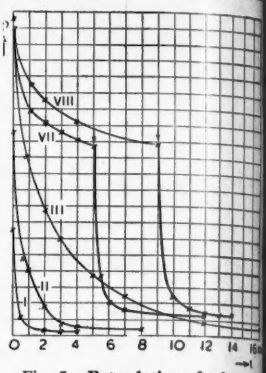

Fig. 5. **Retardation of adsorption of oxygen by reason of increasing charge of gas in tank walls.**

being ignited, in tests VII. and VIII. the mutator was switched in so as to accelerate the adsorbtion.

If the tank walls are cold the pressure at first drops more rapidly than when they are warm. After a few minutes the pressure again rises but upon attaining a certain maximum value, continues its downward trend. With increasing temperature part of the adsorbed gas is again released (Fig. 6).

Though it is true that gas molecules always adhere to the metal surface, the effective forces are not of the same magnitude for different gases. N_2, H_2, CO and CO_2 are not adsorbed until they are ionized by the electric arc. The phenomenon here, therefore, is not the so-called physical adsorption occurring in the case of active carbon at low temperatures. The arc increases the internal energy of the gas molecules which are thus combined more thoroughly by the metallic surface. This has been called activated or chemical adsorption. Should the forces between the gas and metal molecules become still greater, the gas adsorption may lead to the formation of a chemical combination.

Some of the molecules adsorbed by the tank walls are re-evaporated, but are replaced by new molecules. It will be readily understood, therefore, why the temperature of the tank has an influence on the rate of adsorption. At higher temperatures more molecules are evaporated, but if the same number replaces them at the surface of the metal the pressure in the gas chamber will sink less rapidly.

As proved by the above test results, however, the effectiveness of adsorbtion cannot entirely be depended upon in the manufacture of mutators as the adsorption might easily be too highly retarded. Therefore, treatment based on research is necessary during manufacture.

Curve 1 : Mutator cold at beginning of test.
Curve 2 : Mutator warm at beginning of test.
↓ = moment of switching in mutator.

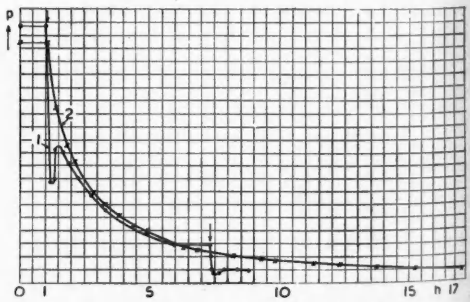

Fig. 6. **Influence of mutator temp. on the adsorption of oxygen**